Numerical computation of the stable and unstable manifolds of saddles of randomly perturbed dynamical systems: An operator approach

Numerical Computation of the Stable and Unstable Manifolds of Saddles of Randomly Perturbed Dynamical Systems: an Operator Approach

Kaio C. B. Benedetti[1,*], Paulo B. Gonçalves[2], Stefano Lenci[3] and Giuseppe Rega[4]

[1]School of Civil and Environmental Engineering, Federal University of Goiás, Goiânia, Brazil

[2]Department of Civil and Environmental Engineering, Pontifical Catholic University of Rio de Janeiro, Rio de Janeiro, Brazil

[3]Department of Civil and Building Engineering, and Architecture, Polytechnic University of Marche, Ancona, Italy

[4]Department of Structural and Geotechnical Engineering, Sapienza University of Rome, Rome, Italy

Abstract: Invariant manifolds are fundamental geometric structures in the field of nonlinear dynamical systems, providing insights into the system's long-term global behavior. In the context of nondeterministic dynamical systems (e.g., stochastic or random dynamical systems), the concept of invariant manifolds generalizes but becomes more nuanced due to the presence of randomness or uncertainty and the definition of invariance must account for the probabilistic behavior. In this work, the theory of measurable dynamics is applied to compute the stable and unstable manifolds distributions and observables of saddles of nondeterministic dynamical systems. First, all necessary definitions are introduced, including the flow map, the transfer operator and its dual in both closed and open spaces, and the classical discretization over the space of constant distributions along with its corresponding dual. Next, invariant manifolds for nondeterministic systems are defined, and a proof of existence is provided for a marginal distribution f_{W_u} over the unstable manifold, along with its dual observable g_{W_s} over the stable manifold. Finally, a discretization strategy for the open-flow transfer operator is presented, along with a method for computing f_{W_u} and g_{W_s}. This theory provides a definition and proof of the existence for both stable and unstable manifolds, based on the spectrum of the open-flow transfer operator. These theoretical concepts are then applied to an electrically actuated microarch, where the effects of noise and damping uncertainty on the distributions of invariant manifolds are demonstrated. In summary, the main contribution of the present work is to employ the theory of measurable dynamics to define and prove the existence of unstable manifold distributions and stable manifold observables via the spectrum of an open-flow transfer operator. In addition, a computational discretization procedure, based on the Ulam method, is introduced alongside analysis of the operator's spectral properties. The results of the electrically actuated microarch reveal three interconnected stochastic phenomena: diminished convergence probability, expansion of the stable manifold across its basin, and fusion of the unstable manifold with the attractor.

Keywords: Global dynamics; transfer operators; stable and unstable manifolds; stochastic dynamics; basin of attraction; electrically actuated microarch.

1 Introduction

The dynamical systems theory is essential for modeling a wide range of natural phenomena. Among the various geometrical structures these systems can exhibit, stable and unstable manifolds associated with saddle solutions are particularly significant, as highlighted in the literature [1, 2]. These invariant manifolds provide structure to the flow of solutions and reveal key characteristics of a system's dynamics [3]. Stable manifolds delimit regions of convergence and act as separatrices for basins of attraction, while unstable manifolds can connect to attractors, infinity, or other saddles, revealing the phase-space flow structure and the decay rates of solutions. The interaction between these manifolds is also critical; for instance, the tangency of stable and unstable manifolds is a well-studied phenomenon that often leads to chaotic behavior and basin erosion [1, 2]. These aspects underscore the importance of invariant manifolds in fully characterizing the underlying global dynamics of a system.

While invariant manifolds are of great importance, computing them is highly challenging. Analytical solutions exist for only a few systems [1], so numerical or semi-analytical strategies are often required. For instance, in systems with fast-slow dynamics, invariant manifolds can be constructed by continuing solutions along the slow variable, treated as a parameter [4, 5]. Autonomous dynamical systems' manifolds can be obtained through an ordered upwind method, a strategy with a relatively low computational cost [6], although it is not parallelizable. For a general time-series, a nonparametric Bayesian approach can be employed to compute the global stable manifold [7]. This method relies solely on time-series data rather than requiring the exact equations of the dynamical system. Over the past decades, this data-focused paradigm has been extensively explored, particularly through the lens of Koopman theory [8] and Perron-Frobenius theory [9], which together form the foundation of measurable dynamics [10].

Many contributions rely solely on the data paradigm. Dellnitz and coworkers [9, 11, 12] developed the subdivision and selection algorithm for computing both stable and unstable manifolds by treating the phase space as a disjoint collection of regions. The underlying idea is that trajectories converge toward the stable or unstable manifold over positive or negative time, respectively. These manifolds can be approximated by identifying regions that remain persistent under backward or forward time integration, resulting in a box-covering of the relevant regions. The algorithm is implemented in the software package GAIO [13], which also supports other dynamical analyses based on the box-covering of the phase space. GAIO provides a robust framework for such computations, making it a valuable tool in the study of dynamical systems. Another strategy, designated as compatible cell-mapping, was proposed by Yue and coworkers. This method can be applied to stable and unstable manifolds of saddles [14] and to global attractors of stochastic dynamical systems [15]. More recently, the authors proposed a different adaptive phase-space discretization, the generalized Ulam method [16, 17], which can be applied to deterministic, stochastic, and parametric uncertainty systems. All three strategies are adaptive phase-space discretization methods that employ a Monte Carlo approximation of the phase-space flow over a disjoint partition

The original data-driven and box-covering of phase space strategy is the classical Ulam method [10], which is used to approximate invariant measures in dynamical systems. It approximates the transfer operator over the phase-space as a Markov matrix P_h through a Monte Carlo approximation of the phase-space flow. This matrix encodes the entire flow structure of the underlying dynamics in phase space, providing critical insights into the system's behavior. From this, Sinai-Bowen-Ruelle measures – specifically, the invariant distributions of attractors over the phase-space – are derived as fixed points of the operator P_h. These fixed points are represented by vectors satisfying the equation $fP_h = f$ (see [9, 18, 19]). Transient analysis also reveals how distributions evolve towards the fixed points of the operator P_h [20, 21]. This analysis can identify P-bifurcations, which occur due to parameter variations and indicate qualitative changes in the stationary distribution. In [22] the extended composite cell coordinate system method is employed to investigate the effects of noise on basins of attraction. Particularly suited for such transfer operator analysis is the concept of committor functions, as defined by Lindner and Hellmann [23], which extends the notion of a region of attraction to stochastic systems.

The remaining spectrum of matrix P_h, $fP_h = \mu f$ for $|\mu| < 1$, encodes how the flow is organized in the phase-space, in particular the functions with μ close to 1. This fact motivated the definition of a corresponding open-flow matrix, $\overline{P}_h$, with fixed points of P_h being removed. As a result, stable and unstable manifolds are encoded into the maximum spectrum of $\overline{P}_h$ [24, 25]. In the transfer operator literature, this spectrum is also referred as almost-invariant sets [9, 26–30].

A key feature of stable and unstable invariant manifolds is that their tangency can signal the presence of chaotic solutions [1, 2]. In particular, for non-autonomous smooth nonlinear systems where the forcing term is periodic, the Melnikov method has proven to be effective in predicting the emergence of chaos [2, 3]. This method involves constructing a function known as the "Melnikov function," which computes the distance between stable and unstable invariant manifolds in the Poincaré map. When this function equals zero, the manifolds intersect transversally, and this intersection is a precursor to chaotic behavior in the system. The Melnikov method thus provides a powerful tool for analyzing the conditions under which chaos arises in dynamical systems.

The theory of stable and unstable invariant manifolds for deterministic dynamics is well developed, with various available strategies for their computation. The theory for nondeterministic dynamical systems is considerably more complex, owing to complications arising from noise or parameter randomness. Arnold [31] presents a comprehensive theory of dynamical systems with noise, including detailed definitions of invariant manifolds. Analyzing these manifolds is not trivial, as they are governed by stochastic processes. In fact, tools designed for deterministic systems, such as the aforementioned Melnikov method, need to be adjusted if they are applied to nondeterministic systems [32–34]. This particular case enables the prediction of stochastic chaos, a phenomenon where the existence of chaotic solutions depends on the sampled noise, making the solutions themselves random processes. This construction is interesting because it bridges deterministic and stochastic chaos. Furthermore, the Melnikov process can be evaluated within the framework of stochastic bifurcation theory, which identifies the parameters at which the system undergoes bifurcations. In contrast to noise-driven systems, the theory for random-parameter dynamics is somewhat simpler. Here, the focus is on a pointwise definition of flows: for each parameter value, a flow map and structure are defined,

distributed according to the parameter space [35]. While this approach simplifies certain aspects, the overall behavior of such systems can still be highly complex, depending on the interplay between parameter variations and system dynamics.

An important advantage of combining the data paradigm with the Ulam method lies in its broad applicability to nondeterministic systems. The Markov matrix representation of the flow, P_h, describes the convergence behavior between different regions in phase-space for a fixed time-step. This approach can be extended to noisy systems using Monte-Carlo computations, which involve sampling initial conditions and integrating them over time [10]. For instance, [10] demonstrates how this method effectively captures the influence of stochastic noise on system dynamics. This principle was extensively applied in the literature, with applications in the detection of transport barriers [36], the analysis of dynamical systems with parameter uncertainty [37], invariant sets of infinite-dimensional dynamical systems [38, 39], and a set-oriented path-following method for computation of parameter-dependent attractors [40]. Other strategies to approximate the Markov matrix P_h had also been investigated, such as applying piecewise linear and quadratic functions [41], higher-order approximations [42], spline [43], least-squares approximation [44], and adaptative phase-space discretization [16, 45]. Strategies based on the Koopman theory can also be considered because of the duality between the transfer and Koopman operators [46]. Cell-mapping methods have been developed as well [14, 15], with applications for nonautonomous systems [21] under colored noise [47], stochastic bifurcations in a turbulent swirling flow [48], and a combination with digraph algorithms [49]. It is worth citing that one main advantage of data-based strategies is the application of high-performance computing [50, 51], reducing the computational time considerably.

The analytical framework of transfer operators and manifold analysis has broad utility in deterministic and stochastic dynamics, as demonstrated by recent research. Siettos and Russo [52] formulated an expansion of stable and unstable manifolds in a polynomial basis over the phase space and adapted this approach for data-driven systems with unknown governing equations using a technique related to the dynamical mode decomposition [46]. Other advances in manifold computation include the use of physics-informed machine learning for their approximation [53]. A major application area combines cell-mapping with deep learning. Building on earlier generalized cell-mapping methods, Yue and colleagues [54–56] have developed this synergy for global analysis, parameter identification, and response prediction of deterministic dynamical systems. This framework has also been used to analyze global dynamics and noise-induced transitions in specific physical systems, such as a two-dimensional panel in flow [57]. Further applications extend also to algorithm design and global manifold learning, with examples including the creation of gradient-free optimization algorithms for hybrid systems [58] and the development of methods to globalize reduced order models from both equations and data [59]. Still, understanding how nondeterminism affects physical models, especially manifolds, requires a proper theoretical framework. The theory of Arnold describes invariant manifolds also as stochastic processes [31], with their behavior depending on the underlying noise. Therefore, there are many invariant manifolds, each with a corresponding noise sample, forming a set that continuously depends on the noise space. The same statement is found in the theory of stochastic invariant manifolds of continuous systems driven by noise, proposed by Chekroun et al. [60]. This behavior points to the existence of a distribution function of invariant manifolds over the phase-space, an object without proper definition or proof in the current literature.

This distribution, if it exists, would quantify the random behavior of the manifolds in the same manner as a random variable is described by its distribution, with statistics readily available from this function. One way to address this issue is to investigate the spectrum of P_h with eigenvalues $|\mu| < 1$, which has been shown in [24, 25] to be connected to both stable and unstable manifolds. Available strategies for computing P_h and its spectrum can be adapted to address invariant manifolds distributions and, since P_h is general for both deterministic and nondeterministic dynamics, they can be applied to stochastic systems.

The analysis of saddle manifolds presents a significant challenge in both deterministic and stochastic dynamics, with numerous numerical and analytical strategies proposed in the literature. However, the prevailing focus has largely been on the sampling of these manifolds, leaving a comprehensive description of their phase-space distribution notably underdeveloped. The present work applies the theory of measurable dynamics to define and prove the existence of both unstable manifold distributions and stable manifold observables from the spectrum of the open-flow transfer operator. These objects are formally constructed, with the distributions residing in the space of piecewise constant functions, $\Delta_h \subset L^1(\mathbb{X})$, and the corresponding observables in dual space, $\Delta_h^* \subset L^\infty(\mathbb{X})$. Then, a computational procedure to obtain their discretization is proposed, based on the classical Ulam method. From the definition of an open-flow operator, properties of its spectra are proven, and a new discretization parameter is proposed. Finally, an electrically actuated microarch [17] is analyzed, where the effects of noise and damping uncertainty over invariant manifolds' distributions are demonstrated. The results illustrate three interconnected phenomena: the loss of convergence probability under stochastic forcing, the expansion of the stable manifold across the stochastic basin, and the merging of the unstable manifold with the attractor.

This work is organized as follows. In Section 2, the theory of transfer operators over open and closed nondeterministic flows is explored. Initially, all necessary definitions are exposed, including the flow map, the transfer operator and its dual in both closed and open spaces, the classical discretization over the space of constant distributions and corresponding dual. Next, invariant manifolds for nondeterministic systems are defined, with proof of existence of a marginal distribution f_{W_u} over the unstable manifold with its dual observable g_{W_s} over the stable manifold. Lastly, a discretization strategy for the open flow transfer operator and computation of both f_{W_u} and g_{W_s} are presented. In Section 3, the results of the previous section are applied to an electrically actuated microarch device. Section 4 presents the final remarks.

2 Nondeterministic dynamics and flow-map structures

2.1 Closed-flow transfer operator general definitions

First, following [16], a general dynamical system defined as

$$\varphi_t: \mathbb{T} \times \Omega \times \mathbb{L} \times \mathbb{X} \to \mathbb{X}, \tag{1}$$

$$(t, \omega, \lambda, \boldsymbol{x}) \mapsto \varphi_t(\theta_t\omega, \lambda, \boldsymbol{x}),$$

is considered, where $\boldsymbol{x} \in \mathbb{X}$, $\mathbb{X}$ is the phase-space (Lebesgue measurable), $t \in \mathbb{T}$ is a time dimension (continuous or discrete), $\omega \in \Omega$ is the noise with evolution governed by θ, and $\lambda \in \mathbb{L}$ is a random parameter. The dependency of φ_t over the nondeterministic parameters θ and λ can be suppressed to $\varphi_t(\boldsymbol{x})$ when the context is clear. For general definitions regarding random dynamical systems, refer to the work of Arnold [31]. Here, it is assumed that there exists at least one invariant or periodic-invariant measure, where $f_{A(\lambda)}(\boldsymbol{x}): \mathbb{X} \to \mathbb{R}^+$ is the probability density function of an attractor $A(\lambda) \in \mathbb{X}$, and a corresponding map of probability of convergence $g_{A(\lambda)}(\varepsilon, \boldsymbol{x}): (0; 1] \times \mathbb{X} \to [0; 1]$ at a time horizon $1/\varepsilon$. Functions $g_{A(\lambda)}(\varepsilon, \boldsymbol{x})$ have the same characteristics of the basin of attraction of $A(\lambda)$, defined by Lindner and Hellmann [23] as generalized committor functions. The attractors are noise-dependent, varying in the phase space $\mathbb{X}$ according to the function $\theta_t\omega$. However, their corresponding distribution $f_{A(\lambda)}$ and generalized committor function $g_{A(\lambda)}$ are defined by marginalizing over the noise space; consequently, they carry no explicit noise argument. This marginalization is not applied to the uncertainty parameter λ, which therefore remains an explicit argument. Furthermore, for conciseness, explicit dependence on the phase-space variable $\mathbb{X}$ will be suppressed throughout the manuscript when clear from context. Thus, $f_{A(\lambda)}(x)$ and $g_{A(\lambda)}(\epsilon, x)$ will be referred to simply as $f_{A(\lambda)}$ and $g_{A(\lambda)}$, respectively, as well as general distributions f and observables g.

Probability densities $f_{A(\lambda)}$ belong to the function space $L^1(\mathbb{X})$. Associated with the dynamical system in Eq. (1) is a transfer operator $\mathcal{P}_t(\lambda)$ acting over $L^1(\mathbb{X})$, defined as [16]

$$\mathcal{P}_t(\lambda): L^1(\mathbb{X}) \to L^1(\mathbb{X}),$$

$$\int_B \mathcal{P}_t(\lambda)[f]\, d\boldsymbol{x} = \int_{\mathbb{X}} \left\{ \int_{\Omega} \mathrm{id}_B\big(\varphi_t(\omega, \lambda, \boldsymbol{x})\big)\, dP_\omega \right\} f\, d\boldsymbol{x}, \tag{2}$$

where $\mathrm{id}_B(\cdot)$ is the indicator function of the set $B \subseteq \mathbb{X}$. According to this formal definition, $\mathcal{P}_t(\lambda)$ operates not only over attractors distributions $f_{A(\lambda)}$, but also over any $f \in L^1(\mathbb{X})$. It is known as the Foias operator [61], a generalization of the Perron-Frobenius operator for stochastic systems. Taking $\Omega = \{\omega\}$ and $\mathbb{L} = \{\lambda\}$ as singleton sets, with $\theta_t\omega = \omega$, and considering the property $\mathrm{id}_B(\varphi_t) = \mathrm{id}_{\varphi_t^{-1}(B)}(\boldsymbol{x})$, where $\varphi_t^{-1}(B)$ is the pre-image of the set B under the dynamics φ_t, reduces the definition (2) to the classical Perron-Frobenius operator,

$$\mathcal{P}_t: L^1(\mathbb{X}) \to L^1(\mathbb{X}),$$

$$\int_B \mathcal{P}_t[f]\, d\boldsymbol{x} = \int_{\varphi_t^{-1}(B)} f\, d\boldsymbol{x}. \tag{3}$$

For both deterministic and nondeterministic systems, $\mathcal{P}_t$ has the following properties [61]:

1. $\mathcal{P}_t[c_1 f_1 + c_2 f_2] = c_1\mathcal{P}_t[f_1] + c_2\mathcal{P}_t[f_2], \forall\, c_1, c_2 \in \mathbb{R},$ (4)

2. $\mathcal{P}_t[f] \geq 0$ if $f \geq 0$,

3. $\int_{\mathbb{X}} \mathcal{P}_t[f]\, d\boldsymbol{x} = \int_{\mathbb{X}} f\, d\boldsymbol{x}$ if $f \geq 0$,

4. $\int_{\mathbb{X}} |\mathcal{P}_t[f]|\, d\boldsymbol{x} \leq \int_{\mathbb{X}} |f|\, d\boldsymbol{x}$.

These are the linearity, the positivity, the integral-preserving, and the contraction properties, respectively. Notice the distinction between the third and fourth properties. While the contraction property is valid for all distributions $f \in L^1(\mathbb{X})$, the integral-preserving property is valid only for positive distributions. For instance, any probability distribution is integral-preserving under the action of $\mathcal{P}_t$, including attractors' distributions $f_{A(\lambda)}$.

The contraction property in Eq. (4) implies that the spectra of $\mathcal{P}_t$ is limited, with radius 1, resulting in eigenfunctions $\phi_{(\lambda)}(\boldsymbol{x})\colon \mathbb{X} \to \mathbb{C}$ with eigenvalues $\mu_{(\lambda)} \in \mathbb{C}$, $|\mu_{(\lambda)}| \leq 1$. In particular, all attractors' distributions, $f_{A(\lambda)}$, are fixed points of $\mathcal{P}_t(\lambda)$, where $\mathcal{P}_t(\lambda)[f_{A(\lambda)}] = f_{A(\lambda)}$. They constitute the fixed space of $\mathcal{P}_t(\lambda)$, that is, $f_{A(\lambda)} \in \text{fix}\{\mathcal{P}_t(\lambda)\}$, having eigenvalue $\mu_{(\lambda)} = 1$. The space $\text{fix}\{\mathcal{P}_t(\lambda)\}$ was the main focus of our previous development [16, 45], discretizing attractors' densities $f_{A(\lambda)}$ and basin observables $g_{A(\lambda)}$.

For the remaining spectra, $|\mu_{(\lambda)}| < 1$, it can be shown that corresponding eigenfunctions $\phi_{(\lambda)}$ have zero L^1-norm. For simplicity, let's consider only the deterministic case, where the eigenproblem is written as $\mathcal{P}_t(\lambda)[\phi_{(\lambda)}] = \mu_{(\lambda)}\, \phi_{(\lambda)}$. As the image of $\phi_{(\lambda)}$ is in the complex plane, $\mathbb{C}$, we define that $\phi_{(\lambda)} = (\phi_{\Re+} + \phi_{\Im+} i) - (\phi_{\Re-} + \phi_{\Im-} i)$, where each component is

$$\begin{aligned} \phi_{\Re+} &= \max(0, \Re[\phi_{(\lambda)}]), \\ \phi_{\Re-} &= \max(0, -\Re[\phi_{(\lambda)}]), \\ \phi_{\Im+} &= \max(0, \Im[\phi_{(\lambda)}]), \\ \phi_{\Im-} &= \max(0, -\Im[\phi_{(\lambda)}]), \end{aligned} \tag{5}$$

$i = \sqrt{-1}$, $\Re[\ \ ]$ is the real part and $\Im[\ \ ]$ is the imaginary part. Then,

$$\begin{aligned} &\int_{\mathbb{X}} \mathcal{P}_t(\lambda)[(\phi_{\Re+} + \phi_{\Im+} i) - (\phi_{\Re-} + \phi_{\Im-} i)]\, d\boldsymbol{x} \\ &\qquad = \mu_{(\lambda)} \int_{\mathbb{X}} [(\phi_{\Re+} + \phi_{\Im+} i) - (\phi_{\Re-} + \phi_{\Im-} i)]\, d\boldsymbol{x}. \end{aligned} \tag{6}$$

Applying the integral-preserving property,

$$\int_{\mathbb{X}} \mathcal{P}_t(\lambda)[\phi_{\Re\pm}]\, d\boldsymbol{x} = \int_{\mathbb{X}} \phi_{\Re\pm}\, d\boldsymbol{x}\,,$$
$$\int_{\mathbb{X}} \mathcal{P}_t(\lambda)[\phi_{\Im\pm}]\, d\boldsymbol{x} = \int_{\mathbb{X}} \phi_{\Im\pm}\, d\boldsymbol{x}, \tag{7}$$

results in

$$\left(1-\mu_{(\lambda)}\right)\int_{\mathbb{X}} \left[(\phi_{\Re+}+\phi_{\Im+}i)-(\phi_{\Re-}+\phi_{\Im-}i)\right]\, d\boldsymbol{x} = 0. \tag{8}$$

The conclusion is that

$$\left|\mu_{(\lambda)}\right| < 1 \Leftrightarrow \int_{\mathbb{X}} \phi_{(\lambda)}\, d\boldsymbol{x} = 0\ \forall \phi_{(\lambda)} \in L^1(\mathbb{X}). \tag{9}$$

The result in [25] is limited to real signed distributions, whereas the result in Eq. (9) applies to all the spectra of $\mathcal{P}_t(\lambda)$ with $\left|\mu_{(\lambda)}\right| < 1$, including complex distributions. Therefore, each complex distribution has an escape rate from its support given by $-\log\left(\left|\mu_{(\lambda)}\right|\right)$, see [25].

The properties discussed so far are applicable to both deterministic and stochastic dynamics. This comes from the fact that both cases are represented by a Markov operator, specifically, the Perron-Frobenius for deterministic and the Foias for stochastic dynamics [61]. Since the only restriction is that $\mathcal{P}_t$ is a Markov operator, the conclusion follows through. It should be clear that distributions $\phi_{(\lambda)}$ with $\left|\mu_{(\lambda)}\right| < 1$ do not quantify uncertainty in the classical sense of a probability distribution. For closed flows discussed so far, the sign of the distribution separates almost invariant regions in the phase-space, see [26], for both deterministic and stochastic dynamics. The true quantification of the flow comes from the analysis of the open-flow dynamics, which will be addressed in the next subsections.

2.2 Classical Ulam discretization of transfer operators and their duals

The discretization of transfer operators over general partitions of the phase-space is based on [16]. It follows the description proposed by Ding et al. [62]: starting from a disjoint partition of the phase-space $\mathbb{X}$ as $\mathbb{B} = \{b_1, \dots, b_i\}$ with characteristic size h, a projection operator Q_h from the space of distributions $L^1(\mathbb{X})$ to the space of piecewise constant functions $\Delta_h = \{\mathbf{1}_1, \dots, \mathbf{1}_i\}$, where $\mathbf{1}_i = \mathrm{id}_{b_i}/m(b_i)$ is a constant density function supported in b_i with measure $m(b_i) = \int_{b_i} d\boldsymbol{x}$, is defined as,

$$Q_h : L^1(\mathbb{X}) \to \Delta_h, \tag{10}$$

$$Q_h[f] = \sum_i \mathbf{1}_i \int_{b_i} f \, d\boldsymbol{x}.$$

The projected transfer operator is obtained as $Q_h[\mathcal{P}_t(\lambda)] = P_h(\lambda)$, that is,

$$\begin{aligned} &P_h(\lambda): \Delta_h \to \Delta_h, \\ &f_h P_h(\lambda) = \sum_{i,j} f_i p_{ij}(\lambda) \mathbf{1}_j, \end{aligned} \tag{11}$$

where $f_h = Q_h[f(\boldsymbol{x})]$. The row vector f_i is

$$f_i = \int_{b_i} f \, d\boldsymbol{x}, \tag{12}$$

and matrix p_{ij} is, considering noise ω and random parameter λ,

$$p_{ij}(\lambda) = \frac{1}{m(b_i)} \int_{b_i} \left\{ \int_{\Omega} \mathrm{id}_{b_j}\big(\varphi_t(\omega, \lambda, \boldsymbol{x})\big) dP_\omega \right\} d\boldsymbol{x}. \tag{13}$$

The dependence on a random parameter λ defines a distribution of discretized transfer operators over $\mathbb{L}$. Global dynamics statistics, such as mean attractors and basins over $\mathbb{L}$, were investigated in [16]. Importantly, while the random parameter λ does not change the dynamics of a specific system over time, it results in a distribution of dynamical systems by extending the pointwise definition introduced by Ashwin [35]. Specifically, there exists a one-to-one mapping between the parameter λ and the dynamics $p_{ij}(\lambda)$, which fully determines the system's behavior. For further details, the reader is referred to [16]. In the deterministic case, this discretization approach reduces to the well-known Ulam method

$$p_{ij} = \frac{m\left(b_i \cap \varphi_t^{-1}(b_j)\right)}{m(b_i)}. \tag{14}$$

For both nondeterministic and deterministic dynamics (Eqs. (13) and (14), respectively), a Monte Carlo strategy can be applied to estimate each entry p_{ij}. This involves sampling elements from each set b_i and performing numerical integration over a single time-step. The key distinction between deterministic and noisy dynamics lies in the numerical integration of $\varphi_t(\omega,\cdot,\cdot)$ and the required sample size of initial conditions in b_i. Specifically, noisy dynamics may require a larger sample size to account for stochastic effects, while deterministic dynamics rely on precise integration methods. For a comprehensive discussion of these techniques, see [37].

The discretized transfer operators p_{ij} in Eqs. (13) and (14) can be understood as Petrov-Galerkin projections [46]. Taking the dual space $\Delta_h^* = \{\mathbf{1}_1^*, \dots, \mathbf{1}_i^*\}$, where $\mathbf{1}_i^* = \mathrm{id}_{b_i}$ is the indicator function of the set $b_i \subset \mathbb{X}$, the Petrov-Galerkin projection of $\mathcal{P}_t$ over Δ_h with test functionals in Δ_h^* is the unique operator $P_h \colon \Delta_h \to \Delta_h$ satisfying the equality

$$\int_{\mathbb{X}} \mathbf{1}_j^* \, \mathcal{P}_t(\lambda)[\mathbf{1}_i] \, d\boldsymbol{x} = \int_{\mathbb{X}} \mathbf{1}_j^* \, \mathbf{1}_i P_h(\lambda) \, d\boldsymbol{x}, \quad \forall \, i, j. \tag{15}$$

In order to apply Eq. (15) and validate the dual space Δ_h^*, it is necessary to define the composition operator, also known as Koopman operator [61]. It acts on the space of observables $L^\infty(\mathbb{X})$, propagating functions $g(\boldsymbol{x}) \in L^\infty(\mathbb{X})$ forward in time along trajectories of the system (1),

$$\begin{aligned} &\mathcal{K}_t(\lambda) \colon L^\infty(\mathbb{X}) \to L^\infty(\mathbb{X}), \\ &\mathcal{K}_t(\lambda)[g] = \int_{\Omega} g \circ \varphi_t(\omega, \lambda, \boldsymbol{x}) \, dP_\omega, \end{aligned} \tag{16}$$

where $\circ$ is the composition operator. Also, taking $\Omega = \{\omega\}$ and $\mathbb{L} = \{\lambda\}$ as singleton sets, with $\theta_t \omega = \omega$, the definition reduces to the deterministic case, i.e.,

$$\begin{aligned} &\mathcal{K}_t \colon L^\infty(\mathbb{X}) \to L^\infty(\mathbb{X}), \\ &\mathcal{K}_t[g] = g \circ \varphi_t(\boldsymbol{x}). \end{aligned} \tag{17}$$

Finally, the adjoint property between $\mathcal{P}_t$ and $\mathcal{K}_t$ can be written as

$$\int_{\mathbb{X}} g \, \mathcal{P}_t(\lambda)[f] \, d\boldsymbol{x} = \int_{\mathbb{X}} \mathcal{K}_t(\lambda)[g] \, f \, d\boldsymbol{x}, \tag{18}$$

and properties in Eq. (4) also apply to $\mathcal{K}_t(\lambda)$. With the definitions of $\mathcal{K}_t(\lambda)$ in Eqs. (16) and (17), the adjoint property, Eq. (18), and the definitions of functions $\mathbf{1}_i$ and $\mathbf{1}_i^*$, the Petrov-Galerkin projection in Eq. (15) can be developed. By expanding the left-hand side of (18), one obtains

$$\begin{aligned} \int_{\mathbb{X}} \mathbf{1}_j^* \, \mathcal{P}_t(\lambda)[\mathbf{1}_i] \, d\boldsymbol{x} &= \int_{\mathbb{X}} \mathcal{K}_t(\lambda)\left[\mathbf{1}_j^*\right] \mathbf{1}_i \, d\boldsymbol{x} \\ &= \int_{\mathbb{X}} \left\{ \int_{\Omega} \mathbf{1}_j^* \circ \varphi_t(\omega, \lambda, \boldsymbol{x}) \, dP_\omega \right\} \mathbf{1}_i \, d\boldsymbol{x} \\ &= \frac{1}{m(b_i)} \int_{b_i} \left\{ \int_{\Omega} \mathrm{id}_{b_j}\big(\varphi_t(\omega, \lambda, \boldsymbol{x})\big) dP_\omega \right\} d\boldsymbol{x}, \end{aligned} \tag{19}$$

which is exactly the definition of matrix $p_{ij}(\lambda)$ given in Eq. (13). The deterministic case is obtained considering $\Omega = \{\omega\}$ and $\mathbb{L} = \{\lambda\}$ as singleton sets, with $\theta_t \omega = \omega$, resulting in Eq. (14). The expansion of the right-hand side of (15) is given by

$$\begin{aligned}
\int_{\mathbb{X}} \mathbf{1}_j^* \, \mathbf{1}_i P_h \, d\boldsymbol{x} &= \int_{\mathbb{X}} \mathbf{1}_j^* \sum_{k,l} \left\{ \int_{b_k} \mathbf{1}_i \, d\boldsymbol{x} \right\} p_{kl} \mathbf{1}_l \, d\boldsymbol{x} \\
&= \int_{\mathbb{X}} \mathrm{id}_{b_j} \sum_{k,l} \left\{ \int_{b_k} \frac{\mathrm{id}_{b_i}}{m(b_i)} d\boldsymbol{x} \right\} p_{kl} \frac{\mathrm{id}_{b_l}}{m(b_l)} d\boldsymbol{x} \\
&= \sum_{l} \left\{ \int_{b_j} p_{il} \frac{\mathrm{id}_{b_l}}{m(b_l)} d\boldsymbol{x} \right\} \\
&= p_{ij},
\end{aligned} \tag{20}$$

where the definition of P_h in Eq. (11) was considered and summation over indexes k, l are canceled by the indicator functions $\mathrm{id}_{b_i}, \mathrm{id}_{b_j}$, contracting as $k = i, l = j$. Therefore, it is shown that the discretized dual space where observable functions g reside is $\Delta_h^* = \{\mathbf{1}_1^*, \dots, \mathbf{1}_i^*\}$, as previously stated. This information will be used in the next section for the computation of discretized global stable manifolds.

As in the case of transfer operators, composition operators can be discretized over the adjoint space Δ_h^*. For this, the projection operator over Δ_h^* is defined as,

$$\begin{aligned}
&Q_h^* : L^\infty(\mathbb{X}) \to \Delta_h^*, \\
&Q_h^*[g] = \sum_i \mathbf{1}_i^* \int_{b_i} \frac{g}{m(b_i)} d\boldsymbol{x}.
\end{aligned} \tag{21}$$

The projected composition operator is obtained as $Q_h^*[\mathcal{K}_t(\lambda)] = K_h(\lambda)$, that is,

$$\begin{aligned}
&K_h(\lambda) : \Delta_h^* \to \Delta_h^*, \\
&K_h(\lambda) g_h = \sum_{i,j} \mathbf{1}_j^* p_{ji}(\lambda) g_i,
\end{aligned} \tag{22}$$

where $g_h = Q_h^*[g]$. The column vector g_i is

$$g_i = \int_{b_i} \frac{g}{m(b_i)} d\boldsymbol{x}, \tag{23}$$

and the matrix $p_{ji}(\lambda)$ is the transpose of the transfer operator in Eq. (13) for nondeterministic dynamics and Eq. (14) for deterministic dynamics. This result is expected since $\mathcal{K}_t(\lambda)$ is the adjoint operator of $\mathcal{P}_t(\lambda)$, and can be summarized as $K_h(\lambda)g_h = P_h^T(\lambda)g_h$ for discretized operators.

2.3 Stable and unstable manifolds of deterministic and nondeterministic dynamics: definitions, and weak and strong convergence in measure

The transfer operator $\mathcal{P}_t$ is a Markov operator that is linear, positive, and integral-preserving [23]. Its matrix discretization p_{ij}, whether deterministic or non-deterministic, is a row-stochastic matrix with a spectral radius equal to one. In previous work, the authors developed strategies to approximate the fixed space fix$\{\mathcal{P}_t\}$, which encodes distributions of attractor densities and their basins [16, 45]. Additionally, the matrix p_{ij} can be used to extract information about the stable and unstable manifolds of the flow φ_t [24]. Building on these works, these concepts are here revised and the analysis expanded from the perspective of function spaces.

Following [24, 25], the starting point is the disjoint partition of the phase-space between attracting regions, i.e., the attractors' supports, and wandering regions. The attractors' supports form a set $\mathbb{H} \subseteq \mathbb{X}$, explicitly defined as $\mathbb{H} = \text{supp}\{\text{fix}\{\mathcal{P}_t(\lambda)\}\}$, see Fig. 1(a). The type of attractor, such as fixed point, periodic, aperiodic, chaotic, or stochastic, is not relevant to this formulation. The complement of $\mathbb{H}$, named $\overline{\mathbb{X}} = \mathbb{X}\backslash\mathbb{H}$, represents all the wandering regions of the phase-space. Then, an open-flow dynamical system is defined in the wandering region as

$$\begin{aligned} &\overline{\varphi}_t : \mathbb{T} \times \Omega \times \mathbb{L} \times \overline{\mathbb{X}} \to \mathbb{X}, \\ &(t, \omega, \lambda, \boldsymbol{x}) \mapsto \overline{\varphi}_t(\theta_t\omega, \lambda, \boldsymbol{x}), \end{aligned} \tag{24}$$

where the same variable definitions for system (1) apply. Fig. 1(b) represents $\overline{\varphi}_t$, with $\partial\mathbb{H}$ being a one-way boundary through which trajectories leave the wandering region $\overline{\mathbb{X}}$ with increasing probability as time increases. Once a trajectory enters $\mathbb{H}$, it cannot return to $\overline{\mathbb{X}}$. The main property of the flow $\overline{\varphi}_t$ is that the pre-image of $\mathbb{H}$ under $\overline{\varphi}_t$ lies within $\overline{\mathbb{X}}$; that is, $\overline{\varphi}_t^{-1}(\mathbb{H}) \subseteq \overline{\mathbb{X}}$. Because the set $\mathbb{H}$ is not in the domain of $\overline{\varphi}_t$, the flow is not defined there. This observation leads directly to the property above. An important and non-standard consequence is that $\overline{\varphi}_t$ cannot have attractors. This is because regions $\mathbb{H}$ that are forward-invariant under the original flow φ_t lie outside the domain of $\overline{\varphi}_t$, which justifies the definition of $\mathbb{H}$ as a "hole" in $\mathbb{X}$

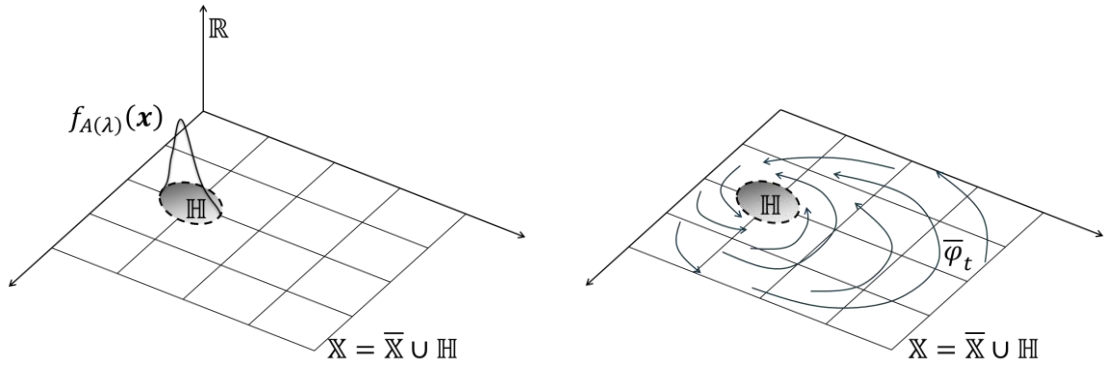

(a) attracting regions $\mathbb{H}$ and wandering regions $\overline{\mathbb{X}}$ (b) open-flow dynamics $\overline{\varphi}_t$

Fig. 1 – Definitions of attracting regions, wandering regions, and open-flow dynamics

Associated with $\overline{\varphi}_t$ is the conditional transfer operator $\overline{\mathcal{P}}_t$ for nondeterministic dynamics defined as

$$\overline{\mathcal{P}}_t(\lambda)\colon L^1(\mathbb{X}) \to L^1(\mathbb{X}),$$
$$\int_B \overline{\mathcal{P}}_t(\lambda)[f]\, d\boldsymbol{x} = \int_{\mathbb{X}} \left\{ \int_{\Omega} \mathrm{id}_B\left(\overline{\varphi}_t(\omega, \lambda, \boldsymbol{x})\right) dP_\omega \right\} f\, d\boldsymbol{x} \tag{25}$$

which can be expanded, following Froyland and Stancevic [25], as

$$\overline{\mathcal{P}}_t\colon L^1(\mathbb{X}) \to L^1(\mathbb{X}),$$
$$\int_B \overline{\mathcal{P}}_t[f]\, d\boldsymbol{x} = \int_{\overline{\varphi}_t^{-1}(B)} f\, d\boldsymbol{x}, \tag{26}$$

for deterministic dynamics, $\forall B \subset \mathbb{X}$, where $\overline{\varphi}_t^{-1}(B)$ is the preimage of B under the action of $\overline{\varphi}_t$. The hole $\mathbb{H}$ implies that the integral-preserving property is no longer true. To see it, consider a density function $\mathbf{1}_{\mathbb{X}}$ supported over the entire phase-space under the action of $\overline{\mathcal{P}}_t$,

$$\int_{\mathbb{X}} \overline{\mathcal{P}}_t[\mathbf{1}_{\mathbb{X}}]\, d\boldsymbol{x} = \int_{\overline{\varphi}_t^{-1}(\mathbb{X})} \mathbf{1}_{\mathbb{X}}\, d\boldsymbol{x}. \tag{27}$$

Since $\overline{\varphi}_{-t}(\mathbb{X}) \subset \overline{\mathbb{X}}$,

$$\int_{\overline{\varphi}_t^{-1}(\mathbb{X})} \mathbf{1}_{\mathbb{X}}\, d\boldsymbol{x} < \int_{\overline{\mathbb{X}}} \mathbf{1}_{\mathbb{X}}\, d\boldsymbol{x} < \int_{\mathbb{X}} \mathbf{1}_{\mathbb{X}}\, d\boldsymbol{x} = 1, \tag{28}$$

resulting in the following inequality,

$$\int_{\mathbb{X}} \overline{\mathcal{P}}_t[\mathbf{1}_{\mathbb{X}}]\, d\boldsymbol{x} < 1. \tag{29}$$

For general distributions with complex image, the contraction property is obtained,

$$\int_{\mathbb{X}} \left|\overline{\mathcal{P}}_t[f]\right| d\boldsymbol{x} < \int_{\mathbb{X}} |f|\, d\boldsymbol{x}. \tag{30}$$

The proof for nondeterministic systems follows the same structure.

As previously demonstrated, eigenfunctions $\phi_{(\lambda)}$ of $\mathcal{P}_t(\lambda)$ with $|\mu_{(\lambda)}| < 1$ satisfy $\int_{\mathbb{X}} \phi\, d\boldsymbol{x} = 0$. However, the same cannot be asserted for $\overline{\mathcal{P}}_t(\lambda)$ due to the lack of an integral-preserving property. Let $\overline{\phi}_{(\lambda)}(\boldsymbol{x})\colon \mathbb{X} \to \mathbb{C}$ be an eigenfunction of $\overline{\mathcal{P}}_t(\lambda)$, that is, $\overline{\mathcal{P}}_t(\lambda)\,\overline{\phi}_{(\lambda)} = \overline{\mu}_{(\lambda)}\,\overline{\phi}_{(\lambda)}$. Only real positive eigenfunctions, $\overline{\phi}_{\Re+}\colon \mathbb{X} \to \mathbb{R}^+$ are considered. Note the distinction between $\overline{\phi}_{\Re+}$, an eigenfunction by itself, and the previous definition in (5), where $\phi_{\Re+}$ is the part of $\phi_{(\lambda)}$ with real and positive image. Integrating the eigenvalue equation over $\mathbb{X}$ yields

$$\int_{\mathbb{X}} \overline{\mathcal{P}}_t(\lambda)[\overline{\phi}_{\Re+}]\, d\boldsymbol{x} = \overline{\mu}_{(\lambda)} \int_{\mathbb{X}} \overline{\phi}_{\Re+}\, d\boldsymbol{x}. \tag{31}$$

By considering the contraction property, Eq. (30),

$$\int_{\mathbb{X}} \overline{\mathcal{P}}_t(\lambda)[\overline{\phi}_{\Re+}]\, d\boldsymbol{x} < \int_{\mathbb{X}} \overline{\phi}_{\Re+}\, d\boldsymbol{x}, \tag{32}$$

and, finally, the following inequality is obtained,

$$0 < \left(1 - \overline{\mu}_{(\lambda)}\right) \int_{\mathbb{X}} \overline{\phi}_{\Re+}\, d\boldsymbol{x}. \tag{33}$$

Recalling that $\left|\overline{\mu}_{(\lambda)}\right| < 1$, the conclusion is that inequality (33) allows for the existence of positive real-valued eigenfunctions $\overline{\phi}_{(\lambda)}$ with corresponding eigenvalues $\overline{\mu}_{(\lambda)} \in \Re_{(-1,1)}$. In contrast, the demonstration of Eq. (9) results in a contradiction if such a positive real distribution exists for $\mathcal{P}_t(\lambda)$, whereas the conditional transfer operator $\overline{\mathcal{P}}_t(\lambda)$ permits their existence.

Another property of the eigenfunctions $\overline{\phi}_{(\lambda)}$ of $\overline{\mathcal{P}}_t(\lambda)$ is that they vanish over $\mathbb{H}$. To prove this, a general eigenfunction of $\overline{\mathcal{P}}_t(\lambda)$ is separated into two components over the domains $\overline{\mathbb{X}}$ and $\mathbb{H}$, that is,

$\overline{\phi}_{(\lambda)} = \overline{\phi}_{(\lambda;\overline{\mathbb{X}})} + \overline{\phi}_{(\lambda;\mathbb{H})}$. Considering the phase-space partition $\mathbb{X} = \overline{\mathbb{X}} \cup \mathbb{H}$, the eigenvalue problem in its integral form consequently splits into separate equations for the domains $\overline{\mathbb{X}}$ and $\mathbb{H}$,

$$\int_{\overline{\mathbb{X}}} \overline{\mathcal{P}}_t(\lambda) \left[\overline{\phi}_{(\lambda;\overline{\mathbb{X}})} + \overline{\phi}_{(\lambda;\mathbb{H})}\right] d\boldsymbol{x} = \overline{\mu}_{(\lambda)} \int_{\overline{\mathbb{X}}} \left\{\overline{\phi}_{(\lambda;\overline{\mathbb{X}})} + \overline{\phi}_{(\lambda;\mathbb{H})}\right\} d\boldsymbol{x}, \tag{34}$$

$$\int_{\mathbb{H}} \overline{\mathcal{P}}_t(\lambda) \left[\overline{\phi}_{(\lambda;\overline{\mathbb{X}})} + \overline{\phi}_{(\lambda;\mathbb{H})}\right] d\boldsymbol{x} = \overline{\mu}_{(\lambda)} \int_{\mathbb{H}} \left\{\overline{\phi}_{(\lambda;\overline{\mathbb{X}})} + \overline{\phi}_{(\lambda;\mathbb{H})}\right\} d\boldsymbol{x}. \tag{35}$$

The preimage of any region in $\mathbb{X}$ under the open-flow is $\overline{\varphi}_t^{-1}(\mathbb{X}) \subset \overline{\mathbb{X}}$, see Eq. (24). Since $\overline{\phi}_{(\lambda;\mathbb{H})} = 0$ over $\overline{\mathbb{X}}$, and applying the transfer operator definition in Eq. (25), the left side of Eq. (34) results in

$$\begin{aligned} \int_{\overline{\mathbb{X}}} \overline{\mathcal{P}}_t(\lambda) \left[\overline{\phi}_{(\lambda;\overline{\mathbb{X}})} + \overline{\phi}_{(\lambda;\mathbb{H})}\right] d\boldsymbol{x} &= \int_{\mathbb{X}} \int_{\Omega} \mathrm{id}_{\overline{\mathbb{X}}}\left(\overline{\varphi}_t(\omega,\lambda,\boldsymbol{x})\right) dP_\omega \left\{\overline{\phi}_{(\lambda;\overline{\mathbb{X}})} + \overline{\phi}_{(\lambda;\mathbb{H})}\right\} d\boldsymbol{x} \\ &= \int_{\mathbb{X}} \int_{\Omega} \mathrm{id}_{\overline{\mathbb{X}}}\left(\overline{\varphi}_t(\omega,\lambda,\boldsymbol{x})\right) dP_\omega \left\{\overline{\phi}_{(\lambda;\overline{\mathbb{X}})}\right\} d\boldsymbol{x}, \end{aligned} \tag{36}$$

while the left side of Eq. (35) results in

$$\begin{aligned} &\int_{\mathbb{H}} \overline{\mathcal{P}}_t(\lambda) \left[\overline{\phi}_{(\lambda;\overline{\mathbb{X}})} + \overline{\phi}_{(\lambda;\mathbb{H})}\right] d\boldsymbol{x} \\ &\quad = \int_{\mathbb{X}} \int_{\Omega} \mathrm{id}_{\mathbb{H}}\left(\overline{\varphi}_t(\omega,\lambda,\boldsymbol{x})\right) dP_\omega \left\{\overline{\phi}_{(\lambda;\overline{\mathbb{X}})} + \overline{\phi}_{(\lambda;\mathbb{H})}\right\} d\boldsymbol{x} \\ &\quad = 0, \end{aligned} \tag{37}$$

since $\mathrm{id}_{\mathbb{H}}\left(\overline{\varphi}_t(\omega,\lambda,\boldsymbol{x})\right) = 0$. Eqs. (36) and (37) imply that $\overline{\mathcal{P}}_t(\lambda)$ acts only on distributions valued over $\overline{\mathbb{X}}$. Finally, expanding the right sides of Eqs. (34) and (35), and considering Eqs. (36) and (37) results in

$$\int_{\mathbb{X}} \int_{\Omega} \mathrm{id}_{\overline{\mathbb{X}}}\left(\overline{\varphi}_t(\omega,\lambda,\boldsymbol{x})\right) dP_\omega \, \overline{\phi}_{(\lambda;\overline{\mathbb{X}})} \, d\boldsymbol{x} = \overline{\mu}_{(\lambda)} \int_{\overline{\mathbb{X}}} \overline{\phi}_{(\lambda;\overline{\mathbb{X}})} \, d\boldsymbol{x}, \tag{38}$$

$$\int_{\mathbb{H}} \overline{\phi}_{(\lambda;\mathbb{H})} \, d\boldsymbol{x} = 0. \tag{39}$$

since $\overline{\phi}_{(\lambda;\overline{\mathbb{X}})} = 0$ over $\mathbb{H}$. Restricting to the case where $m(\mathbb{H}) = \int_{\mathbb{H}} d\boldsymbol{x} > 0$, Eqs. (38) and (39) shows that all eigenfunctions $\overline{\phi}_{(\lambda)}$ of $\overline{\mathcal{P}}_t(\lambda)$ vanish over $\mathbb{H}$, as stated earlier. However, cases where $m(\mathbb{H}) = 0$ are not uncommon, with the main example being a fixed-point attractor of a deterministic system. To address this issue, a numerical strategy is proposed in subsection 2.4. Finally, the leading eigenvalue of $\overline{\mathcal{P}}_t(\lambda)$ with real value $0 < \overline{\mu}_{(\lambda)} < 1$ and positive eigenfunction $\int_{\mathbb{X}} \overline{\phi}_{(\lambda)}\, d\boldsymbol{x} > 0$ is the so-called eigenvalue of the measure $dM = \overline{\phi}_{(\lambda)} d\boldsymbol{x}$ in $\mathbb{X}$ with respect to $\overline{\mathbb{X}}$. The rate of escape from $\overline{\mathbb{X}}$ to $\mathbb{H}$ is given by $-\log \overline{\mu}_{(\lambda)}$ [25], extended here to systems with nondeterministic parameter λ with measure P_λ over $\mathbb{L}$.

The conditional transfer operator $\overline{\mathcal{P}}_t(\lambda)$ is considered in the definitions of distributions of globally unstable manifolds and observables of globally stable manifolds, respectively. The existence of a nondeterministic saddle is assumed, here identified as $\boldsymbol{x}_p(\omega, \lambda)$, with positive measure $f_{\boldsymbol{x}_p(\lambda)}(\boldsymbol{x})$ in $\mathbb{X}$, that is, $\int_{\mathbb{X}} f_{\boldsymbol{x}_p}\, d\boldsymbol{x} = 1$. The deterministic case, where stable and unstable manifolds of $\boldsymbol{x}_P$ are denoted $W_s(\boldsymbol{x}_p)$ and $W_u(\boldsymbol{x}_p)$, has been extensively investigated in the literature, with definitions available in [1, 29]. In contrast, for stochastic systems, the definitions differ, as discussed in Chapter 7 of [31]. To address this difference, recall that $\boldsymbol{x}_p(\omega, \lambda)$ is a random point in $\mathbb{X}$. Consequently, the sets of points converging to $\boldsymbol{x}_p$ forward or backward in time also become random, that is, $W_s(\boldsymbol{x}_p) \mapsto W_s(\boldsymbol{x}_p, \omega, \lambda)$ and $W_u(\boldsymbol{x}_p) \mapsto W_u(\boldsymbol{x}_p, \omega, \lambda)$. As random objects, these manifolds are described by probability distributions over the phase space, denoted f_{W_s} and f_{W_u}. The physical observation of f_{W_s} and f_{W_u} is only possible indirectly through Monte Carlo or statistical analysis, like any random experiment. In practice, the sampling of f_{W_s} requires backward time evolution, making it preferable to obtain the dual of f_{W_u}, that is, the observable g_{W_s}. Since W_s and W_u are random, it is natural to inquire how these objects are distributed and observed in the phase-space $\mathbb{X}$. This section formally defines the distribution f_{W_u} and observable g_{W_s}. A discretization strategy through the Ulam method is discussed in the following subsection.

In the nondeterministic setting, the definitions of stable and unstable manifolds are extended as follows: they are regions of $\mathbb{X}$ that converge, with probability one, to $x_p(\omega, \lambda)$ in forward and backward time, respectively:

$$W_s(\boldsymbol{x}_p, \omega, \lambda) = \left\{\boldsymbol{x} \in \mathbb{X} | P_\omega \left(\lim_{n\to\infty} \overline{\varphi}_t^n(\omega, \lambda, \boldsymbol{x}) = \boldsymbol{x}_p(\omega, \lambda) \right) = 1 \right\}, \tag{40}$$

$$W_u(\boldsymbol{x}_p, \omega, \lambda) = \left\{\boldsymbol{x} \in \mathbb{X} | P_\omega \left(\lim_{n\to\infty} \overline{\varphi}_{-t}^n(\omega, \lambda, \boldsymbol{x}) = \boldsymbol{x}_p(\omega, \lambda) \right) = 1 \right\}. \tag{41}$$

For simplicity, their arguments will be suppressed hereafter with W_s and W_u referring to the stable and unstable manifolds, Eqs. (40) and (41), respectively. Initially, the unstable manifold is addressed. An important question is what the marginal distribution of W_u over $\overline{\mathbb{X}}$ is. To investigate this, a weaker form of convergence is considered, namely, the weak convergence of measures, as defined in [61],

$$\lim_{n\to\infty}\int_{\mathbb{X}} g\, f_n(\lambda,\boldsymbol{x})\, d\boldsymbol{x} = \int_{\mathbb{X}} g\, f_{\boldsymbol{x}_p(\lambda)}\, d\boldsymbol{x}, \qquad \forall\, g \in L^\infty(\mathbb{X}), \tag{42}$$

where g are observables in the dual space $L^\infty(\mathbb{X})$, and $f_n \in L^1(\mathbb{X})$ form a sequence of distributions. To verify Eq. (42), the value of λ is prescribed and a sequence of iterated distributions $f_n \equiv f_n(\lambda,\boldsymbol{x})$ is formed via the open-flow $\overline{\varphi}_t^n$, with $\boldsymbol{x}_p(\omega,\lambda) \notin \mathbb{H}$, that is, $f_n(\lambda,\boldsymbol{x}) = \overline{\mathcal{P}}_t^n(\lambda)[f_0]$. It can be shown that the closed-flow operator $\mathcal{P}_t(\lambda)$ produces a distinct distribution $f_n'(\lambda,\boldsymbol{x})$, whose support lies entirely within $\mathbb{H}$, independently of the choice of f_0. For this reason, the open-flow operator $\overline{\mathcal{P}}_t(\lambda)$ must be employed in place of $\mathcal{P}_t(\lambda)$. Therefore, the limit is expanded as

$$\begin{aligned}
&\lim_{n\to\infty}\int_{\mathbb{X}} g\, \overline{\mathcal{P}}_t^n(\lambda)[f_0]\, d\boldsymbol{x} = \int_{\mathbb{X}} g\, \overline{\mathcal{P}}_t^n(\lambda)\left[f_{\boldsymbol{x}_p(\lambda)}\right] d\boldsymbol{x},\\
&\lim_{n\to\infty}\int_{\mathbb{X}} \left\{\int_{\Omega} g\circ\overline{\varphi}_t^n(\omega,\lambda,\boldsymbol{x})\, dP_\omega\right\} f_0\, d\boldsymbol{x} = \int_{\mathbb{X}} \left\{\int_{\Omega} g\circ\overline{\varphi}_t^n(\omega,\lambda,\boldsymbol{x})\, dP_\omega\right\} f_{\boldsymbol{x}_p(\lambda)}\, d\boldsymbol{x},
\end{aligned} \tag{43}$$

where the duality property of $\overline{\mathcal{P}}_t(\lambda)$ and $\overline{\mathcal{K}}_t(\lambda)$ was considered, as in Eq. (18). Taking the limit $n \to \infty$ results in

$$\begin{aligned}
&\int_{\mathbb{X}} \left\{\int_{\Omega} g\circ\boldsymbol{x}_p(\omega,\lambda)\, dP_\omega\right\} f_0\, d\boldsymbol{x} = \int_{\mathbb{X}} \left\{\int_{\Omega} g\circ\boldsymbol{x}_p(\omega,\lambda)\, dP_\omega\right\} f_{\boldsymbol{x}_p(\lambda)}\, d\boldsymbol{x},\\
&\mathbb{E}_\omega\left[g\left(\boldsymbol{x}_p(\omega,\lambda)\right)\right]\int_{\mathbb{X}} f_0\, d\boldsymbol{x} = \mathbb{E}_\omega\left[g\left(\boldsymbol{x}_p(\omega,\lambda)\right)\right]\int_{\mathbb{X}} f_{\boldsymbol{x}_p(\lambda)}\, d\boldsymbol{x},\\
&\int_{\mathbb{X}} f_0\, d\boldsymbol{x} = \int_{\mathbb{X}} f_{\boldsymbol{x}_p(\lambda)}\, d\boldsymbol{x},
\end{aligned} \tag{44}$$

where $\mathbb{E}_\omega[\cdot]$ is the expectation operator over P_ω. The last equality in Eq. (44) is trivial since both f_0 and $f_{\boldsymbol{x}_p(\lambda)}$ are positive $L^1(\mathbb{X})$ distributions. Consequently, a positive distribution $f_0 \in L^1(\mathbb{X})$ exists which, when iterated under the conditional Perron-Frobenius operator $\overline{\mathcal{P}}_t(\lambda)$, forms a sequence of positive distributions f_n that converges weakly in measure to $f_{\boldsymbol{x}_p(\lambda)}$.

Now, consider the strong convergence in measure given in [61],

$$\lim_{n\to\infty}\left|\int_B f_n(\lambda,\boldsymbol{x})\, d\boldsymbol{x} - \int_B f_{\boldsymbol{x}_p(\lambda)}\, d\boldsymbol{x}\right| = 0, \forall B \subset \mathbb{X}. \tag{45}$$

Considering $f_n(\lambda, \boldsymbol{x}) = \overline{\mathcal{P}}_t^n(\lambda)[f_0(\boldsymbol{x})]$ and $f_{\boldsymbol{x}_p(\lambda)} = \overline{\mathcal{P}}_t^n(\lambda)\left[f_{\boldsymbol{x}_p(\lambda)}\right]$, and that Eq. (45) is also valid for the unitary partition, $B = \mathbb{X}$, Eq. (45) leads to

$$\lim_{n\to\infty}\left|\int_{\mathbb{X}} \overline{\mathcal{P}}_t^n(\lambda)[f_0]\,d\boldsymbol{x} - \int_{\mathbb{X}} \overline{\mathcal{P}}_t^n(\lambda)\left[f_{\boldsymbol{x}_p(\lambda)}\right]d\boldsymbol{x}\right|,$$

$$\lim_{n\to\infty}\left|\int_{\mathbb{X}}\left\{\int_{\Omega} \mathrm{id}_{\mathbb{X}}\left(\overline{\varphi}_t^n(\omega,\lambda,\boldsymbol{x})\right)dP_\omega\right\}f_0\,d\boldsymbol{x}\right. \tag{46}$$

$$\left. - \int_{\mathbb{X}}\left\{\int_{\Omega} \mathrm{id}_{\mathbb{X}}\left(\overline{\varphi}_t^n(\omega,\lambda,\boldsymbol{x})\right)dP_\omega\right\}f_{\boldsymbol{x}_p(\lambda)}\,d\boldsymbol{x}\right|,$$

where the definition of $\overline{\mathcal{P}}_t(\lambda)$, Eq. (25), was applied. Taking the limit $n \to \infty$ results in the pull-back of f_0 to $\mathrm{id}_{\mathbb{X}}\left(\boldsymbol{x}_p(\omega,\lambda)\right)$, that is,

$$\left|\int_{\mathbb{X}}\left\{\int_{\Omega} \mathrm{id}_{\mathbb{X}}\left(\boldsymbol{x}_p(\omega,\lambda)\right)dP_\omega\right\}f_0\,d\boldsymbol{x} - \int_{\mathbb{X}}\left\{\int_{\Omega} \mathrm{id}_{\mathbb{X}}\left(\boldsymbol{x}_p(\omega,\lambda)\right)dP_\omega\right\}f_{\boldsymbol{x}_p(\lambda)}\,d\boldsymbol{x}\right|,$$

$$\left|\int_{\mathbb{X}} \mathrm{id}_{\mathbb{X}}\left(\mathbb{E}_\omega\left[\boldsymbol{x}_p(\omega,\lambda)\right]\right)f_0\,d\boldsymbol{x} - \int_{\mathbb{X}} \mathrm{id}_{\mathbb{X}}\left(\mathbb{E}_\omega\left[\boldsymbol{x}_p(\omega,\lambda)\right]\right)f_{\boldsymbol{x}_p(\lambda)}\,d\boldsymbol{x}\right|, \tag{47}$$

$$\left|\int_{\mathbb{X}} f_0\,d\boldsymbol{x} - \int_{\mathbb{X}} f_{\boldsymbol{x}_p(\lambda)}\,d\boldsymbol{x}\right|,$$

since $\mathbb{E}_\omega[\cdot]$ is the expectation operator of the measure P_ω and $\mathbb{E}_\omega\left[\boldsymbol{x}_p(\omega,\lambda)\right] \in \mathbb{X}$. Therefore, both integrals result in one in the last line of Eq. (47), resulting in zero. Therefore, $f_0 \in L^1(\mathbb{X})$ also converges strongly in measure to $f_{\boldsymbol{x}_p(\lambda)}$ when iterated under $\overline{\mathcal{P}}_t(\lambda)$.

The distribution f_0 can be expanded in the space of real positive eigenfunctions $\overline{\phi}_{i,(\lambda)}$ of $\overline{\mathcal{P}}_t(\lambda)$, with eigenvalues $0 < \overline{\mu}_{i,(\lambda)} < 1$. Thus, $f_0 = \sum_{i=1}^{\infty} v_i \overline{\phi}_{i,(\lambda)}$, with coefficients $v_i \geq 0$. Taking that $\overline{\mathcal{P}}_t(\lambda)\overline{\phi}_{i,(\lambda)} = \overline{\mu}_{i,(\lambda)}\overline{\phi}_{i,(\lambda)}$ there is a decay under the action of $\overline{\mathcal{P}}_t(\lambda)$, with rate given by $-\log \mu_{i,(\lambda)}$. As already mentioned, given a parameter $\lambda \in \mathbb{L}$, the largest eigenvalue μ_i gives the minimum rate of escape from $\overline{\mathbb{X}}$ towards $\mathbb{H}$. The marginal distribution $f_{W_u}(\lambda)$ of $\int_\Omega W_u(\boldsymbol{x}_p, \omega, \lambda)P_\omega$ over $\overline{\mathbb{X}}$ is the corresponding eigenfunction. This definition is general, being applicable to both deterministic and nondeterministic systems. The final mean distribution $f_{W_u} = \mathbb{E}_\lambda\left[f_{W_u}(\lambda)\right]$ over $\mathbb{X}$ is obtained through simple integration,

$$f_{W_u} = \int_{\mathbb{L}} f_{W_u}(\lambda)\, dP_\lambda = \int_{\mathbb{L}} \overline{\phi}_{1,(\lambda)}\, dP_\lambda. \tag{48}$$

The definition of $W_s(\boldsymbol{x}_p, \omega, \lambda)$ is trickier than the previous case. A distribution $f_{W_s}(\lambda)$ can only be obtained through the backward open flow $\overline{\varphi}_{-t}$, which would require a construction of another transfer operator $\overline{\mathcal{P}}_{-t}(\lambda)$, a difficult task since the operator $\overline{\mathcal{P}}_t(\lambda)$ is not, in general, invertible. There are strategies for the construction of an invertible operator to address this issue, see [29] for deterministic dynamics. Nevertheless, it is possible to define an observable function over the stable manifold $g_{W_s}(\lambda)$ from the forward transfer operator $\overline{\mathcal{P}}_t(\lambda)$. Expanding a general observable $g_0 \in L^\infty(\mathbb{X})$ in the dual of the space positive eigenfunctions of $\overline{\mathcal{P}}_t(\lambda)$, that is, $g_0 = \sum_i u_i\, \overline{\phi}^*_{i,(\lambda)}$, and applying $\overline{\mathcal{K}}^n_t(\lambda)$ to both sides, one obtains, using the definition in Eq. (16) and taking that it is a linear operator satisfying properties 1 and 2 in Eq. (4),

$$\overline{\mathcal{K}}^n_t(\lambda)[g_0] = \sum_i u_i\, \overline{\mathcal{K}}^n_t(\lambda)\left[\overline{\phi}^*_{i,(\lambda)}\right],$$

$$\int_\Omega g_0 \circ \overline{\varphi}^n_t(\omega, \lambda, \boldsymbol{x})\, dP_\omega = \sum_i u_i\, \overline{\mu}^n_i(\lambda)\, \overline{\phi}^*_{i,(\lambda)}, \tag{49}$$

$$\sum_i u_i \int_\Omega \overline{\phi}^*_{i,(\lambda)} \circ \overline{\varphi}^n_t(\omega, \lambda, \boldsymbol{x})\, dP_\omega = \sum_i u_i\, \overline{\mu}^n_i(\lambda)\, \overline{\phi}^*_{i,(\lambda)},$$

where $u_i \in \mathbb{R}^+$ and $\overline{\phi}^*_{i,(\lambda)}$ are eigenfunctions of $\overline{\mathcal{K}}_t(\lambda)$ in the space $L^\infty(\mathbb{X})$. Taking the limit $n \to \infty$, the expression reduces to

$$\mathbb{E}_\omega\left[\overline{\phi}^*_{i,(\lambda)}\left(\boldsymbol{x}_p(\omega, \lambda)\right)\right] = \overline{\mu}^n_i(\lambda)\, \overline{\phi}^*_{i,(\lambda)}. \tag{50}$$

Since $|\overline{\mu}_i(\lambda)| < 1$ and $|\overline{\mu}_i(\lambda)| > |\overline{\mu}_{i+1}(\lambda)|$, the right side of Eq. (50) decays to zero for $n \to \infty$. The first mode exhibits the slowest rate of decay within the spectrum of $\overline{\mathcal{K}}_t(\lambda)$ from $\overline{\mathbb{X}}$ to $\mathbb{H}$. Given that $\overline{\mu}_{1,(\lambda)}$ is the leading eigenvalue, $g_{W_s}(\lambda)$ is defined as the corresponding eigenfunction $\overline{\phi}^*_{1,(\lambda)}$ in the dual space $L^\infty(\mathbb{X})$, in direct analogy with the definition of $f_{W_u}(\lambda)$. This definition will enable a simpler discretization in the spaces Δ_h and Δ^*_h. For mean observables, where $g_{W_s} = \mathbb{E}_\lambda[g_{W_s}]$ over $\mathbb{X}$, the measure P_λ is applied,

$$g_{W_s} = \int_{\mathbb{L}} g_{W_s}(\lambda)\, dP_\lambda = \int_{\mathbb{L}} \overline{\phi}^*_{1,(\lambda)}\, dP_\lambda. \tag{51}$$

2.4 Discretization of the open-flow transfer operator and computation of $f_{W_u}(\lambda)$ and $g_{W_s}(\lambda)$

Consider again a disjoint partition of the phase-space $\mathbb{X}$ as $\mathbb{B} = \{b_1, \dots, b_i\}$ with characteristic size h. Taking Q_h as defined in Eq. (10), the projected conditional transfer operator is obtained as $Q_h[\overline{\mathcal{P}}_t(\lambda)] = \overline{P}_h(\lambda)$:

$$\begin{aligned} &\overline{P}_h(\lambda): \Delta_h \to \Delta_h, \\ &f_h \overline{P}_h(\lambda) = \sum_{i,j} f_i \overline{p}_{ij}(\lambda) \mathbf{1}_j, \end{aligned} \tag{52}$$

where $f_h = Q_h[f(\boldsymbol{x})]$ and the row vector f_i is as defined in (12). The conditional transfer matrix $\overline{p}_{ij}(\lambda)$ is given by, for nondeterministic dynamics,

$$\overline{p}_{ij}(\lambda) = \frac{1}{m(b_i)} \int_{b_i} \left\{ \int_{\Omega} \mathrm{id}_{b_j} \left(\overline{\varphi}_t(\omega, \lambda, \boldsymbol{x}) \right) dP_\omega \right\} d\boldsymbol{x}. \tag{53}$$

and for deterministic dynamics,

$$\overline{p}_{ij} = \frac{m\left(b_i \cap \overline{\varphi}_t^{-1}(b_j)\right)}{m(b_i)}, \tag{54}$$

where the only difference of Eq. (53) from Eq. (13) and Eq. (54) from (14) is the open-flow dynamics, $\overline{\varphi}_t$, as defined in Eq. (24). The definition for the projected conditional composition operator is obtained from $Q_h^*[\overline{\mathcal{K}}_t(\lambda)] = \overline{P}_h^T(\lambda)$, resulting in the same conditional transfer matrix $\overline{p}_{ij}(\lambda)$ as in Eqs. (53) and (54).

The definitions in Eqs. (24), (53) and (54) are resumed in a relationship between $\overline{p}_{ij}(\lambda)$ and $p_{ij}(\lambda)$,

$$\overline{p}_{ij}(\lambda) = \begin{cases} p_{ij}(\lambda), & \forall b_i \subset \overline{\mathbb{X}}, \forall b_j \subset \mathbb{X} \\ 0, & \forall b_i \subseteq \mathbb{H}, \forall b_j \subset \mathbb{X}. \end{cases} \tag{55}$$

Definition (55) differs from the one proposed by Klünker et. al. [24]. While in [24] the conditional transfer matrix is defined by setting to zero both rows and columns of $p_{ij}(\lambda)$ corresponding to $\mathbb{H}$, here only the rows are set to zero. The justification comes by examining the definitions of $\overline{p}_{ij}(\lambda)$. Consider two boxes, $b_i \subset \mathbb{X}$ and $b_j \subset \mathbb{X}$. Because the preimage of $\overline{\mathbb{X}}$ is $\overline{\varphi}_t^{-1}(\overline{\mathbb{X}}) \not\subseteq \mathbb{H}$ by definition, the value of $\overline{p}_{ij}(\lambda)$ depends if either b_i or b_j are in $\mathbb{H}$ or $\overline{\mathbb{X}}$. The result is

$$\int_{b_i}\left\{\int_{\Omega}\mathrm{id}_{b_j}\left(\overline{\varphi}_t(\omega,\lambda,\boldsymbol{x})\right)dP_\omega\right\}d\boldsymbol{x}=\begin{cases}r\geq 0, & \forall b_i\subset\overline{\mathbb{X}},\forall b_j\subseteq\mathbb{H},\\ r\geq 0, & \forall b_i\subset\overline{\mathbb{X}},\forall b_j\subset\overline{\mathbb{X}},\\ 0, & \forall b_i\subseteq\mathbb{H},\forall b_j\subseteq\mathbb{H},\\ 0, & \forall b_i\subseteq\mathbb{H},\forall b_j\subset\overline{\mathbb{X}},\end{cases}\tag{56}$$

for nondeterministic dynamics, and

$$m\left(b_i\cap\overline{\varphi}_t^{-1}(b_j)\right)=\begin{cases}r\geq 0, & \forall b_i\subset\overline{\mathbb{X}},\forall b_j\subseteq\mathbb{H},\\ r\geq 0, & \forall b_i\subset\overline{\mathbb{X}},\forall b_j\subset\overline{\mathbb{X}},\\ 0, & \forall b_i\subseteq\mathbb{H},\forall b_j\subseteq\mathbb{H},\\ 0, & \forall b_i\subseteq\mathbb{H},\forall b_j\subset\overline{\mathbb{X}},\end{cases}\tag{57}$$

for deterministic dynamics. In summary, $\overline{p}_{ij}(\lambda)=p_{ij}(\lambda)$ if $b_i\subset\overline{\mathbb{X}}$ and $\overline{p}_{ij}(\lambda)=0$ if $b_i\subseteq\mathbb{H}$, validating Eq. (55). In fact, the open-flow operator $\overline{P}_h(\lambda)$ is a discretization of the conditional transfer operator proposed by Froyland and Stancevic [25], also extended here to random parameters and noise cases.

The open flow operator $\overline{P}_h(\lambda)$ is constructed from the original operator $P_h(\lambda)$ and its invariant distributions $f_{A(\lambda)}$. It should be observed that the original strategy in [24] assumes that attractor sets b_i are such that $p_{ii}(\lambda)=1$, which is based only on the discrete setting. However, it can miss periodic, quasi-periodic, and chaotic attractors, since their distributions are spread over many sets b_i, all with $p_{ii}(\lambda)<1$, as demonstrated by Lasota and Mackey [61], and by Hsu [63]. This is also problematic for stochastic systems, where attractors are diffused over large regions of the phase-space, as shown by Sun and Hsu [64]. Therefore, the boxes that cover the entire support of the attractors' distributions, $\mathrm{supp}\{f_{A(\lambda)}\}$, are considered, allowing other types of attractors to be analyzed. Still, it was observed that if $f_{A(\lambda)}$ is too concentrated (having a small covering over $\mathbb{X}$), then its vicinity could behave as a long transient in the discrete space, hindering the manifold identification. Theoretical justification for this phenomenon comes from analyzing the spectrum of $\overline{\mathcal{P}}_t(\lambda)$ over $\mathbb{H}$. According to Eq. (39), the spectrum of $\overline{\mathcal{P}}_t(\lambda)$ will be zero only if $\mathbb{H}$ is a measurable subset of $\mathbb{X}$ with positive measure, that is, $m(\mathbb{H})>0$. Fixed-point attractors violate this condition, as a single point has zero measure, $m(\{\boldsymbol{x}_p\})=0$. Consequently, the spectrum of $\overline{\mathcal{P}}_t(\lambda)$ can contain Dirac distributions centered on $\mathbb{H}$. In a discrete approximation, these Dirac measures correspond to any probability measure concentrated on a single partition element b_i. To prevent such spectral artifacts, a regularization parameter c is introduced. This parameter effectively enlarges the support of the attractors, thereby ensuring the measurability of $\mathbb{H}$.

The process starts by verifying if an attractor's distribution $f_{A(\lambda)}$ is too concentrated. This is checked by the ratio between the measures of the distribution's support and of the phase-space window,

$$m\left(\mathrm{supp}\left(f^{(k)}\right)\right)>c\,m(\mathbb{X}),\tag{58}$$

$$c \geq \frac{\min m(b_i)}{m(\mathbb{X})},$$

where $f^{(0)} = Q_h\left[\sum f_{A(\lambda)}\right]$ in the first iteration with $\sum f_{A(\lambda)}$ being the sum of all attractors' distributions, $\min m(b_i)$ is the minimum measure of the phase-space partition b_i, and $m(\mathbb{X})$ is the phase-space window measure. If condition (58) is false, given a predefined value c, then $f^{(k)}$ is backpropagated through the Koopman operator, that is, $f^{(k+1)} = P_h^T(\lambda) f^{(k)}$, and condition (58) is evaluated again. This process repeats until the condition is satisfied. Then, the box-covering of the attracting region is defined as $\mathbb{H} = \text{supp}\left(f^{(k)}\right)$, and the i^{th} lines of $\overline{p}_{ij}(\lambda)$ corresponding to $\mathbb{H}$ are set to zero. All other entries of $\overline{p}_{ij}(\lambda)$ are identical to $p_{ij}(\lambda)$, satisfying Eq. (55). The algorithm is summarized in Table 1. At the end, an open-flow discretized transfer operator $\overline{P}_h(\lambda)$ is constructed.

Table 1– Construction of open-flow discrete transfer matrix $\overline{p}_{ij}$

0.	Take $k = 0$, $f^{(k)} = Q_h\left[\sum f_{A(\lambda)}\right]$
1.	Evaluate condition (58). If true, then go to 3, else continue
2	Backpropagate $f^{(k)}$ through the Koopman operator, $f^{(k+1)} = P_h^T(\lambda) f^{(k)}$. Set $k \coloneqq k + 1$ and go to step 1
3.	Define $\mathbb{H} = \text{supp}\left(f^{(k)}\right)$
4.	Define $\overline{p}_{ij}(\lambda) = p_{ij}(\lambda)$. Next, set to zero its i^{th} lines corresponding to $b_i \subseteq \mathbb{H}$

The eigenvalues $\overline{\mu}_{(\lambda)}$ of $\overline{P}_h(\lambda)$ are equal to those of $P_h(\lambda)$, with the exception of the fixed space, where $\mu_{(\lambda)} = 1$. Spectral analysis of $\overline{P}_h(\lambda)$ follows, where the left-eigenvectors with largest real $\overline{\mu}_{(\lambda)}$ are the discretizations of $f_{W_u}(\lambda)$ over Δ_h, and corresponding right-eigenvectors are the discretizations of $g_{W_s}(\lambda)$ over Δ_h^*. The correspondence between the left and right spectra of $\overline{P}_h(\lambda)$ and $\overline{\mathcal{P}}_t(\lambda)$ is easy to check. First, the general eigenvalue problem of $\overline{\mathcal{P}}_t(\lambda)$ is projected over Δ_h,

$$Q_h\left[\overline{\mathcal{P}}_t(\lambda) f_{W_u}(\lambda)\right] = Q_h\left[\overline{\mu}_{(\lambda)} f_{W_u}(\lambda)\right]. \tag{59}$$

Then, considering the projected distribution, Eq. (10), and the projected conditional transfer operator, Eq. (52), the following matrix left eigenvalue problem is obtained,

$$\sum_{i,j} f_i(\lambda) \overline{p}_{ij}(\lambda) \mathbf{1}_j = \overline{\mu}_{(\lambda)} \sum_i \mathbf{1}_i f_i(\lambda), \tag{60}$$

where each entry $f_i(\lambda)$ is

$$f_i(\lambda) = \int_{b_i} f_{W_u}(\lambda)\, d\boldsymbol{x}. \tag{61}$$

Therefore, isolated solutions of Eq. (60) with highest $\overline{\mu}_{(\lambda)}$ will be discretizations of the unstable manifolds' distributions $f_{W_u}(\lambda)$ over Δ_h. The analysis of the right spectra of $\overline{P}_h(\lambda)$ is considered through the general eigenvalue problem of the Koopman operator, projecting it over Δ_h^*,

$$Q_h^*\left[\overline{\mathcal{K}}_t(\lambda)g_{W_s}(\lambda)\right] = Q_h^*\left[\overline{\mu}_{(\lambda)}g_{W_s}(\lambda)\right]. \tag{62}$$

Then, considering the projected observable, Eq.(23), and the projected conditional transfer operator, Eq. (52), the following matrix right eigenvalue problem is obtained,

$$\sum_{i,j} \mathbf{1}_j^* \overline{p}_{ji}(\lambda) g_i(\lambda) = \overline{\mu}_{(\lambda)} \sum_i \mathbf{1}_i^* g_i(\lambda), \tag{63}$$

where each entry $g_i(\lambda)$ is

$$g_i(\lambda) = \int_{b_i} \frac{g_{W_s}(\lambda)}{m(b_i)} d\boldsymbol{x}. \tag{64}$$

Therefore, isolated solutions of Eq. (63) with highest $\overline{\mu}_{(\lambda)}$ will be discretizations of the stable manifolds' observables $g_{W_s}(\lambda)$ over Δ_h^*. Computationally, once the transfer matrix $\overline{p}_{ij}(\lambda)$ is obtained, its left-eigenvectors $f_i(\lambda)$ and right-eigenvectors $g_i(\lambda)$ with highest $\overline{\mu}_{(\lambda)}$ are calculated, approximating $f_{W_u}(\lambda)$ and $g_{W_s}(\lambda)$, respectively. The ease with which both stable and unstable manifolds are derived from the given transfer matrix $p_{ij}(\lambda)$ validates the definitions of $f_{W_u}(\lambda)$ and $g_{W_s}(\lambda)$ in the previous section. This approach also enables a direct extension for stochastic dynamics, since $p_{ij}(\lambda)$ represents both the Perron-Frobenius, Eq. (14), and the Foias operator, Eq. (13). Finally, systems with parametric uncertainty are analyzed through mean distributions and observables, computed via Eqs. (48) and (51), respectively.

Two points must be emphasized. First, following the analysis in the previous section, function $f_{W_u}(\lambda)$ is a positive distribution over $L^1(\mathbb{X})$, and $g_{W_s}(\lambda)$ is a positive observable over $L^\infty(\mathbb{X})$. The graphical representation of each case is different: $f_{W_u}(\lambda)$ is normalized as $\left\|f_{W_u}(\lambda)\right\|_1 = 1$, while $g_{W_s}(\lambda)$ is normalized as $\left\|g_{W_s}(\lambda)\right\|_\infty = 1$. This distinction is expected, since these functions belong to different spaces, and the same occurs for their discretizations $f_i(\lambda)$ and $g_i(\lambda)$. Second, there can exist more isolated positive eigenvalues $\overline{\mu}_{(\lambda)}$. Such cases correspond to the existence of multiple isolated stable and unstable manifolds, as reported by Klünker et. al. [24]. This is no problem for the analysis, being dealt with ease by usual numerical eigensolvers, such as Spectra C++, available at https://spectralib.org/.

3 Random manifolds of a microarch device

In [17] the authors investigated the effect of uncertainties and noise on the nonlinear global dynamics of a micro-electro-mechanical arch obtained from an imperfect microbeam under axial load and electric excitation, using an operator approach. The microarch was assumed to be shallow and modeled using a nonlinear Bernoulli–Euler beam theory and was discretized by the Galerkin method using as interpolating function the linear vibration modes. Then, from the discretized multi degree of freedom model, an accurate single degree of freedom reduced order model, based on theory of nonlinear normal modes, was derived. Here the random stable and unstable manifolds of the electrically actuated microarch are investigated, considering the sdof nonlinear reduced order model (ROM) reported in [17]. Assuming a direct actuation voltage $V_{dc} = 0.7V$, the equations of motion of the deterministic system are given by

$$
\begin{aligned}
&\frac{d}{dt}w_1 = \dot{w}_1,\\
&\frac{d}{dt}\dot{w}_1 = 5.0854w_1^5 + 14.3037w_1^4 - 2.4554\times10^{-6}\dot{w}_1^4 + 0.0035\dot{w}_1^2\\
&\qquad - (121.6181 + 0.0224\dot{w}_1^2)w_1^3 + (762.4990 - 0.0114\dot{w}_1^2)w_1^2\\
&\qquad - (1385.5761 - 0.0172\dot{w}_1^2 + 1.5913\times10^{-5}\dot{w}_1^4)w_1 - c_1\dot{w}_1\\
&\qquad + (c_1 - c_2)[-0.0104w_1\dot{w}_1 - 0.1449\dot{w}_1\\
&\qquad + (0.0351w_1^4 + 1.0034\times10^{-5}w_1^2\dot{w}_1^2)\dot{w}_1\\
&\qquad + (0.0164w_1^2 + 6.5676\times10^{-7}\dot{w}_1^2)w_1\dot{w}_1\\
&\qquad - (0.0193w_1^2 - 5.2796\times10^{-6}\dot{w}_1^2)\dot{w}_1]\\
&\qquad + V_{ac}[0.6280 + 1.0091\times10^{-5}w_1^2\dot{w}_1^2 + 0.0399w_1^4 + 0.098w_1^3\\
&\qquad + 7.2601\times10^{-6}w_1\dot{w}_1^2 + 1.0335\times10^{-6}\dot{w}_1^2 + 0.2257w_1^2 + 0.4405w_1]\\
&\qquad + V_{ac}^2[0.07w_1^3 + 5.1858\times10^{-6}w_1\dot{w}_1^2 + 0.1612w_1^2 + 7.3821\times10^{-7}\dot{w}_1^2\\
&\qquad + 0.3146w_1 + 0.4486],
\end{aligned}
\tag{65}
$$

where w_1 and $\dot{w}_1$ are modal amplitude and velocity of the nonlinear ROM, $(w_1, \dot{w}_1) = (0,0)$ is the energy local minimum, $c_1 = 2\xi\omega_1$ and $c_2 = 2\xi\omega_2$ are damping coefficients of the first and second linear symmetric modes, with ξ as the damping ratio, and $V_{ac} = A\cos(\Omega\, t)$ is the alternating current (AC) actuation. The first and second natural frequencies are $\omega_1 = 37.7$ and $\omega_2 = 116.8$. For completeness, deterministic global dynamics results are reported first.

In [17], two softening resonance regions were observed, one at $\Omega = 37.2$ and other at $\Omega = 18.6$. The former corresponds to the first mode natural frequency, while the latter is a superharmonic resonance. The superharmonic resonance is more prominent, with larger displacement values. So, the superharmonic resonance region was investigated here, considering a forcing frequency $\Omega = 15$ and amplitude of excitation $A = 17V$. The fourth order Runge-Kutta integrator is adopted for the construction of the flow φ_T, with time-step $T/2000$, where T is the period of excitation, $T = 2\pi/\Omega$.

The analyzed phase-space window is $\mathbb{X} = \{-2,3\} \otimes \{-70,60\}$, which contains all the relevant attractors. An adaptative phase-space discretization proposed in [16] was applied, with a starting subdivision of 32 boxes in each dimension. The changes in the basins of attraction and escape region topology with the damping ratio ξ are shown in Fig. 2, together with the corresponding attractors. For $\xi = 0.05$, the two basins are robust, with well-defined smooth boundaries. As the damping ratio decreases, both basins' integrity degrades, with escape tongues gradually eroding them, and the resonant basin being more affected than the nonresonant one. Note that the phase-space discretization of the operator approach entails small numerical diffusion (red color grades) along classical deterministic boundaries. According to Ulam, in the limit of infinity resolution, the method converges to the expected sharp boundaries. The internal saddle is represented by a blue dot in all cases. As basins degrade, the internal saddle moves along the boundary, and at $\xi = 0.01$, it is located at a triple point where the resonant, nonresonant, and escape basins meet.

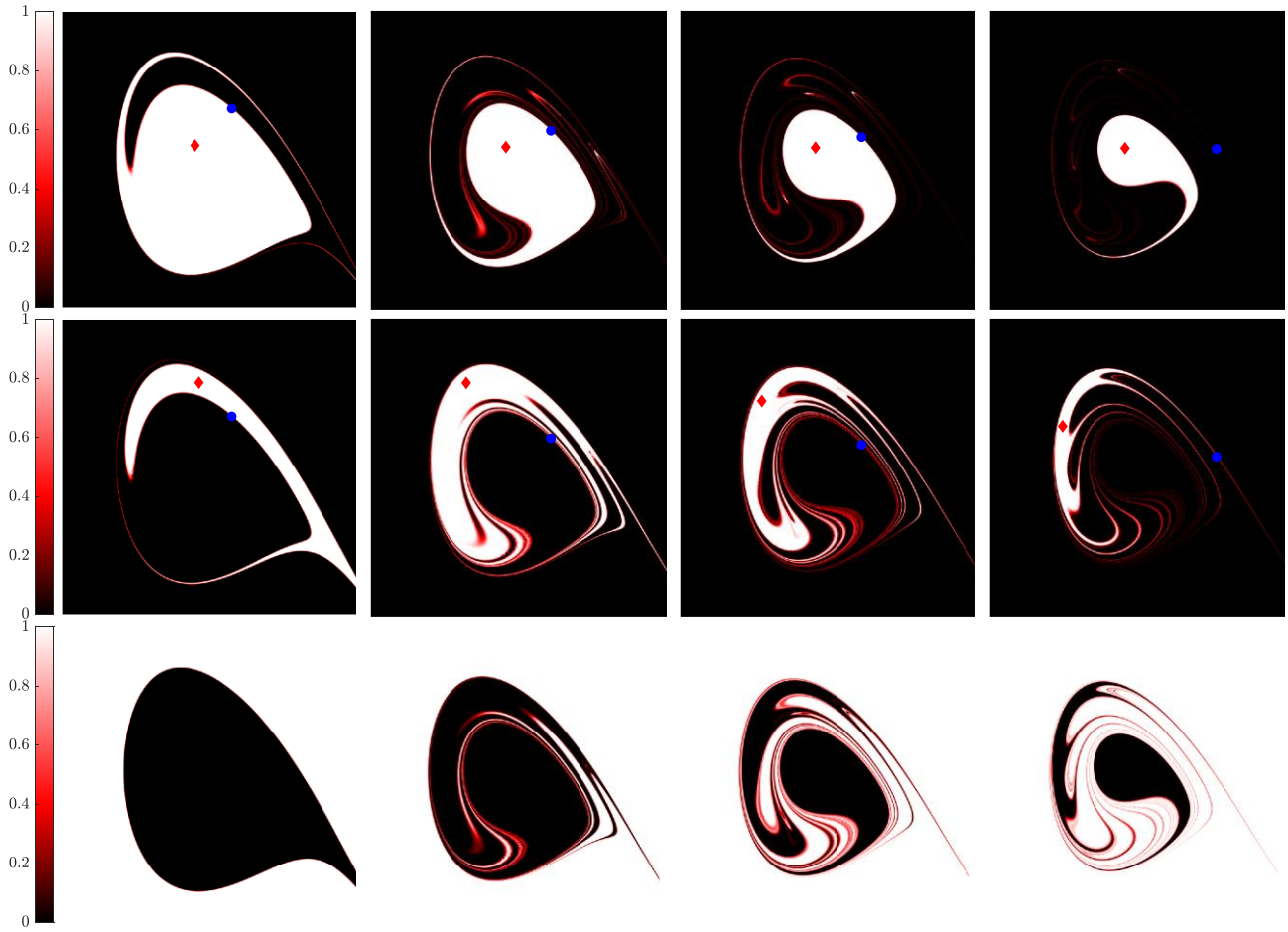

(a) $\xi = 0.05$ (b) $\xi = 0.03$ (c) $\xi = 0.02$ (d) $\xi = 0.01$

Fig. 2 – Deterministic system. Basins' dependency on the critical damping ratio ξ, for $A = 17V$ and $\Omega = 15$, in $(w_1, \dot{w}_1) \in \{-2,3\} \otimes \{-70,60\}$. Attractors marked in red, saddle points marked in blue. First row: nonresonant region, second row: resonant region, third row: escape region.

Fig. 3 illustrates the evolution of the unstable manifold distribution, f_{W_u}, and the stable manifold observable, g_{W_s}, for the saddle point on the basin boundary as the damping ratio decreases. For ξ = 0.05 (Fig. 3a), the manifolds exhibit their simplest form, which aligns with the smooth basin boundaries seen in Fig. 2a. As the damping ratio decreases (Fig. 3b-d), the manifolds grow increasingly

complex. The stretching and folding of the stable manifold, visible in panels 3(a.1-d.1), lead to greater basin fractality and heightened sensitivity to initial conditions near the boundaries. These effects would be further amplified by the introduction of noise. Similarly, the unstable manifolds that converge to the two attractors also develop a more intricate structure with reduced damping, as shown in panels 3(a.2-d.2). Fig. 3b, in particular, reveals variations in density within the manifolds. These density fluctuations reflect the underlying flow structure, indicating that certain branches are more dynamically significant than others. Regions farther from the attractor generally exhibit lower density, forming the tail of the distribution.

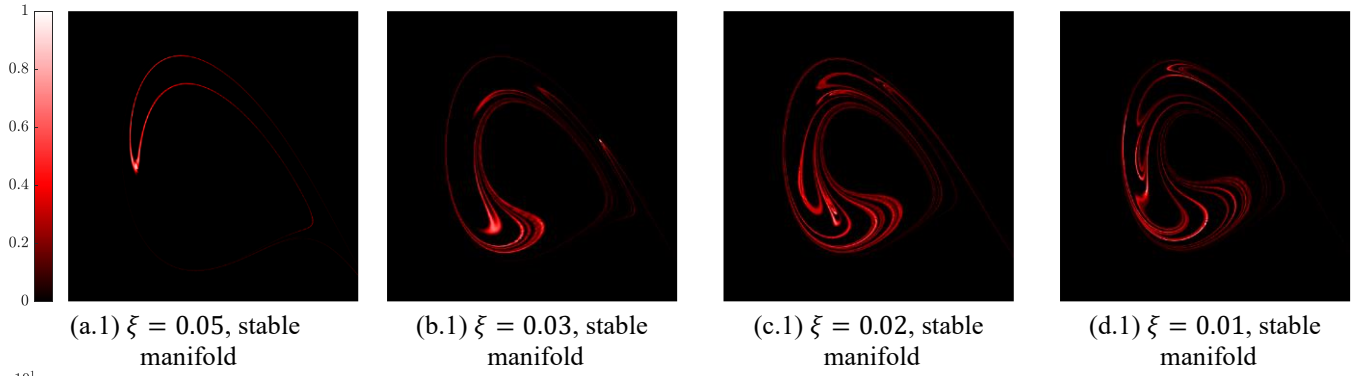

(a.1) $\xi = 0.05$, stable manifold | (b.1) $\xi = 0.03$, stable manifold | (c.1) $\xi = 0.02$, stable manifold | (d.1) $\xi = 0.01$, stable manifold

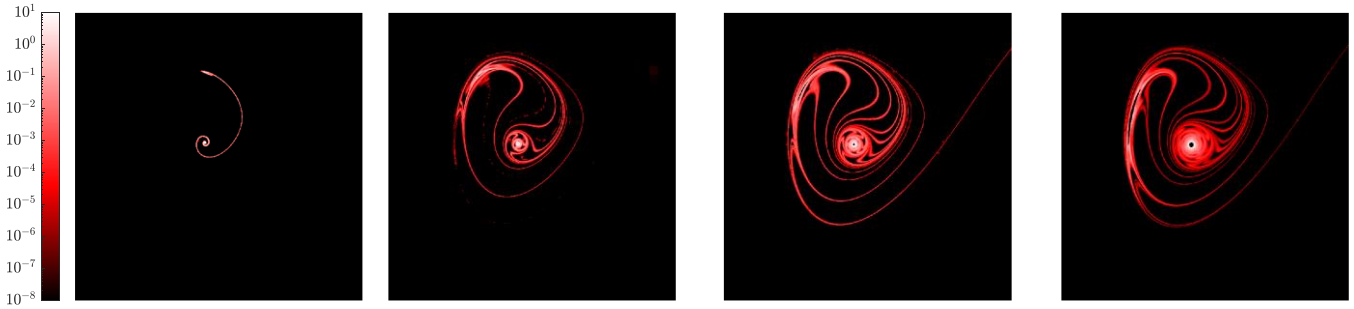

(a.2) $\xi = 0.05$, unstable manifold | (b.2) $\xi = 0.03$, unstable manifold | (c.2) $\xi = 0.02$, unstable manifold | (d.2) $\xi = 0.01$, unstable manifold

Fig. 3 – Deterministic system. Dependency of the stable manifold observable g_{W_s} and unstable manifold distribution f_{W_u} on the critical damping ratio ξ, in $(w_1, \dot{w}_1) \in \{-2,3\} \otimes \{-70,60\}$. $A = 17V$, $\Omega = 15$

Fig. 4(1) shows the intersection of the stable (blue) and unstable (green) manifold supports, known as the *saddle support*, highlighted in red. For low damping ratios, numerous transverse intersections are observed, making visible the presence of a topological horseshoe. These findings demonstrate that the damping coefficient, a parameter often difficult to determine, plays a significant role in shaping the system's global dynamics. The proposed methodology is validated in Fig. 4(2). Using the box-covering algorithm from the software GAIO [13], both stable and unstable manifolds were traced. Qualitatively, the results from both methods agree, with differences restricted to the tail regions of the distribution (i.e., areas of low density). Due to the adaptive phase-space discretization, these tail regions are not always marked for refinement. This results in the gaps visible as green squares, primarily in Fig. 4(b.1). While the refinement criteria can be adjusted to resolve these regions, this comes at the cost of increased computational expense. A qualitative convergence analysis was conducted to balance this trade-off, comparing three levels of phase-space sampling with 10^2, 20^2, and 30^2 initial conditions per box in the initial subdivision (Fig. 5). It was found that 20^2 initial conditions

provided an optimal compromise between result quality and computational cost, and this value was adopted for the study.

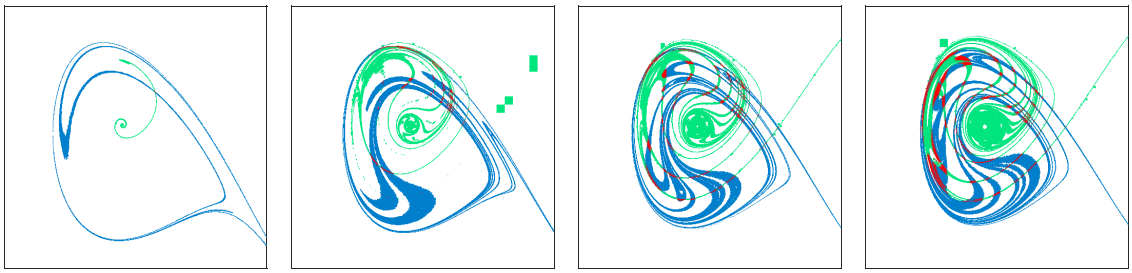

(a.1) $\xi = 0.05$, Ulam method | (b.1) $\xi = 0.03$, Ulam method | (c.1) $\xi = 0.02$, Ulam method | (d.1) $\xi = 0.01$, Ulam method

(a.2) $\xi = 0.05$, box covering | (b.2) $\xi = 0.03$, box covering | (c.2) $\xi = 0.02$, box covering | (d.2) $\xi = 0.01$, box covering

Fig. 4 – Stable (blue), and unstable (green) manifolds' support for varying damping ratio ξ, with intersections marked as red. 1) Ulam method, 2) box-covering, in $(w_1, \dot{w}_1) \in \{-2,3\} \otimes \{-70,60\}$. $A = 17V$, $\Omega = 15$

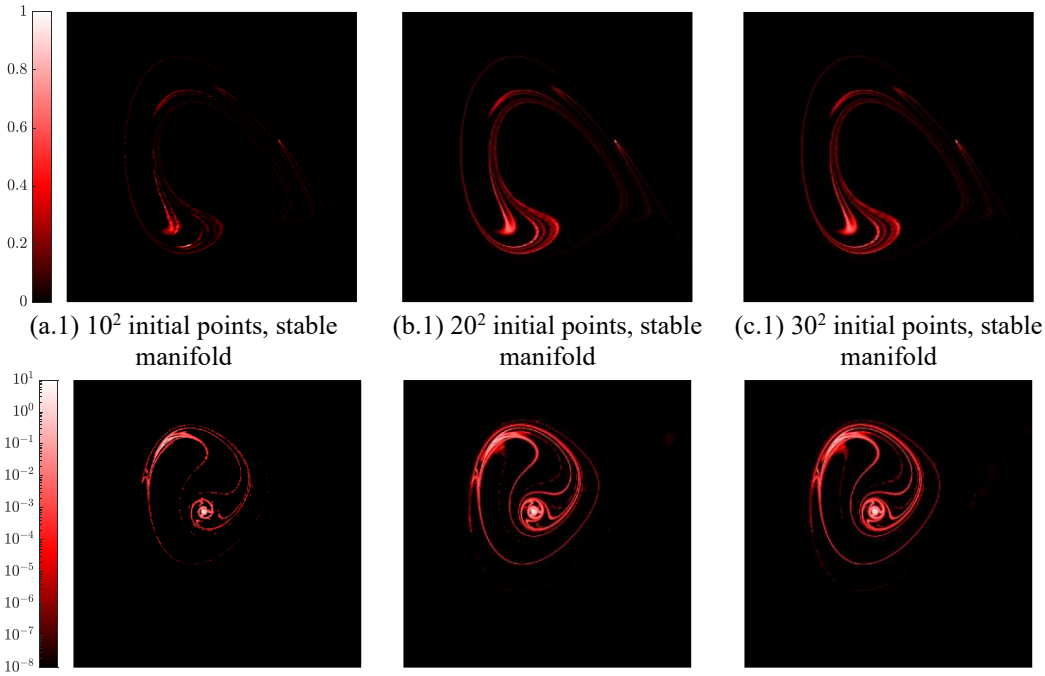

(a.1) 10^2 initial points, stable manifold | (b.1) 20^2 initial points, stable manifold | (c.1) 30^2 initial points, stable manifold

(a.2) 10^2 initial points, unstable manifold | (b.2) 20^2 initial points, unstable manifold | (c.2) 30^2 initial points, unstable manifold

Fig. 5 – Convergence of stable manifold observable g_{W_s} and unstable manifold distribution f_{W_u} with the number of initial integration points per box in $(w_1, \dot{w}_1) \in \{-2,3\} \otimes \{-70,60\}$. $\xi = 0.03$, $A = 17V$, $\Omega = 15$

The necessity of the proposed localization correction in Eq. (58) and Table 1 is demonstrated in Fig. 6. Here, the nonresonant attractor's support is very small, represented by only a single box in the

discretized phase-space. This example contrasts two scenarios: one without support expansion (Fig. 6(a)) and another with it (Fig. 6(b)). Without the support expansion, the numerical method fails to correctly capture the distribution of the unstable manifold and the observable of the stable manifold. This inaccuracy arises from both numerical and analytical limitations, specifically from the phase-space discretization, the flow approximation, and the constraints of considering only Dirac measures on $\mathbb{X}$. The issue is effectively resolved by implementing a simple minimal support expansion within the Ulam discretization framework, as shown here.

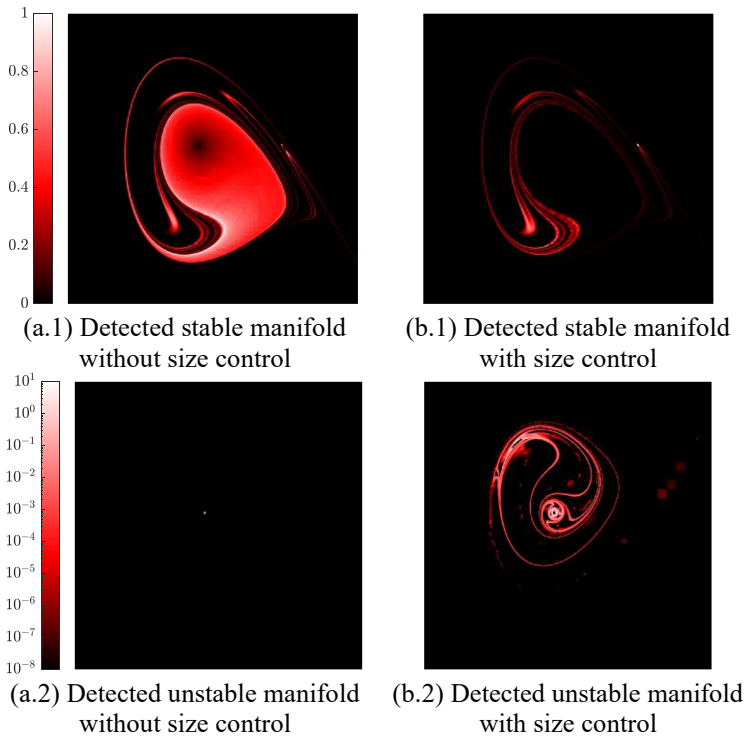

(a.1) Detected stable manifold without size control

(b.1) Detected stable manifold with size control

(a.2) Detected unstable manifold without size control

(b.2) Detected unstable manifold with size control

Fig. 6 – Algorithm comparison with and without measure support control. Stable manifold observable g_{W_s} and unstable manifold distribution f_{W_u} for $\xi = 0.03026093$, $A = 17V$, $\Omega = 15$, in $(w_1, \dot{w}_1) \in \{-2{,}3\} \otimes \{-70{,}60\}$.

Noise effects over the stable and unstable manifolds and the flow structures in phase-space are investigated next. By adding the term $\sigma\dot{W}$ to the right side of the second equation in (65), where $\dot{W}$ is a white noise and σ is a control parameter, a system of stochastic differential equations is obtained. In [17], the superharmonic resonance region where $\Omega = 15$, $A = 17V$, and $\xi = 0.03$ was investigated with varying σ-values, where a stochastic bifurcation was reported for $\sigma = 1.6$. Here, results for $\sigma = 1.5$ are investigated. In Fig. 7, basins of attraction for increasing time horizons $1/\varepsilon$ are depicted. A loss of basin region is observed for $\varepsilon \leq 10^{-9}$. For comparison, [17] observed this loss at a smaller time horizon, with $\varepsilon \leq 10^{-7}$. The difference points to an inverse correlation between the time horizon and the noise intensity: the mean escape time of a solution decreases as noise intensity increases. However, an analysis based solely on basins is insufficient to identify a stochastic bifurcation.

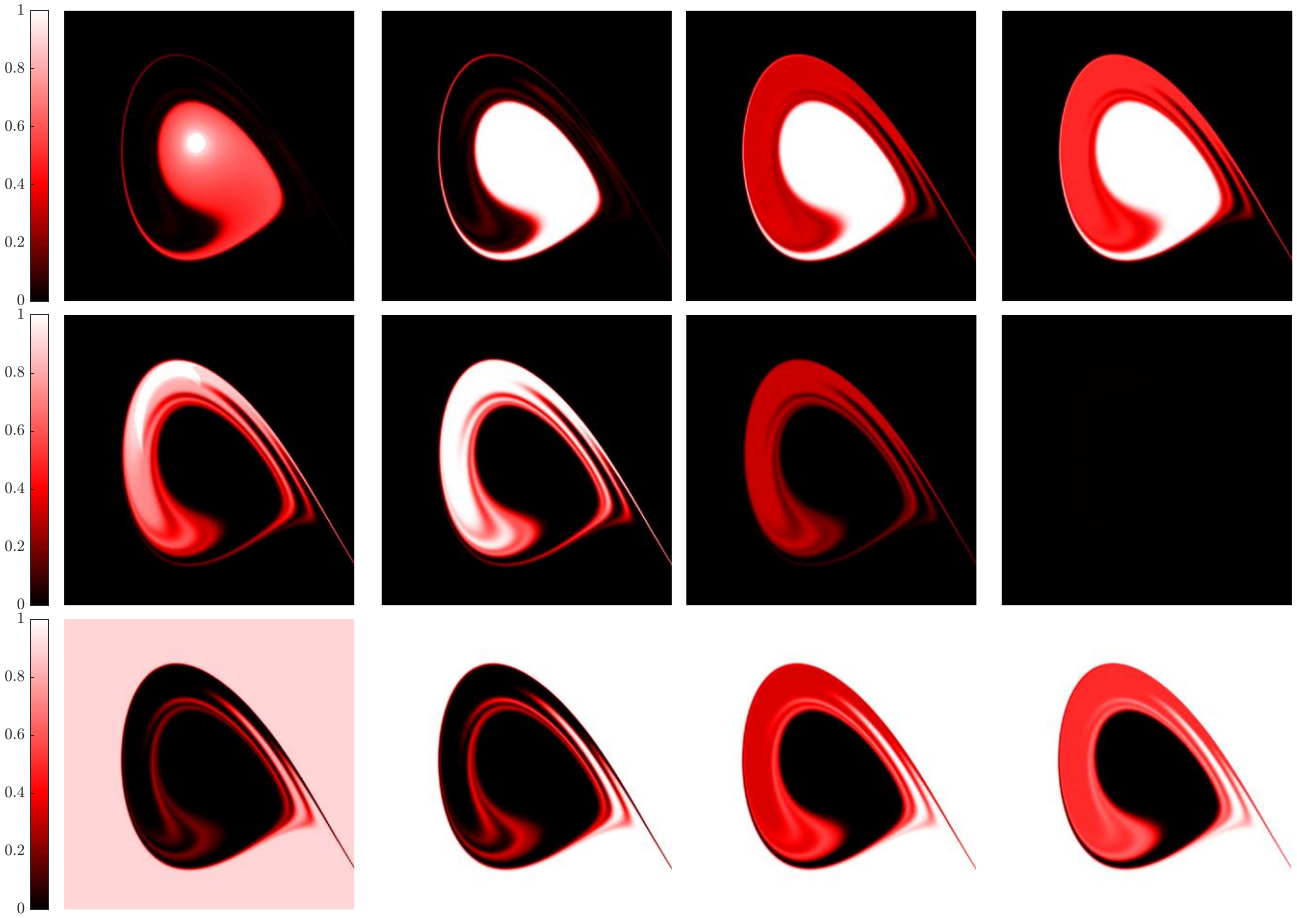

(a) $\varepsilon = 10^{-1}$ (b) $\varepsilon = 10^{-5}$ (c) $\varepsilon = 10^{-9}$ (b) $\varepsilon = 10^{-11}$

Fig. 7 – System with noise. Dependency of the nonresonant (first row), resonant (second row), and escape (third row) region of convergence (color bar) onto the time-horizon $1/\varepsilon$, in $(w_1, \dot{w}_1) \in \{-2,3\} \otimes \{-70,60\}$. $A = 17V$, $\Omega = 15$, $\xi = 0.03$, $\sigma = 1.5$

Fig. 8 illustrates the evolution of the stable manifold observable, g_{W_s}, and the unstable manifold distribution, f_{W_u}, under increasing noise levels. As noise intensifies, both g_{W_s} and f_{W_u} diffuse across the phase space, indicating a loss of certainty in the flow. The unstable manifold is particularly affected; the distinct tongues observed in the deterministic case (Fig. 3(b.2)) spread until they are no longer distinguishable from one another (Fig. 8(d.2)). At $\sigma = 2.0$, a value beyond the stochastic bifurcation point, drastic changes are observed. The stable manifold observable coalesces over the entire resonant region, while the unstable manifold distribution merges with the resonant attractor. Although the eigenvalues $\overline{\mu}$ for g_{W_s} and f_{W_u} remain close to the deterministic value of 0.5467 when $\sigma < 2$, the case of $\sigma = 2.0$ reveals a loss of stability in the attractor measure, signaled by an eigenvalue of $\mu = 0.999996642$. This eigenvalue signifies the formation of a quasi-stationary distribution, shown in Fig. 8(d.2), which arises from the merging of an attractor distribution f_A and the unstable manifold distribution f_{W_u}, the latter being signaled by the eigenvalue $\bar{\mu} = 0.999967$ of the open-flow transfer operator. Precisely identifying this phenomenon is computationally complex and highly dependent on phase-space refinement and flow representation. The adopted Ulam method [16] requires a formal convergence analysis, but current results indicate that the discretization still strongly influences the outcomes. Accurately depicting all system attractors and manifolds necessitates a sufficiently fine phase-space discretization and a high-fidelity flow representation.

The results also illustrate how noise affects the features of the attractors, changing the structure of the unstable and stable manifolds and the homoclinic tangencies (HTs), a topic rarely investigated in the technical literature [65]. The trajectory of the unstable manifold is driven out of the neighborhood of the attractor by noise over a certain number of iterations, causing considerable local deformation of the attractor (formation of "tails"). These are observed in the increasing diffusion of the unstable manifold over its tongues before the bifurcation, Fig. 8(a.2, b.2, c.2).

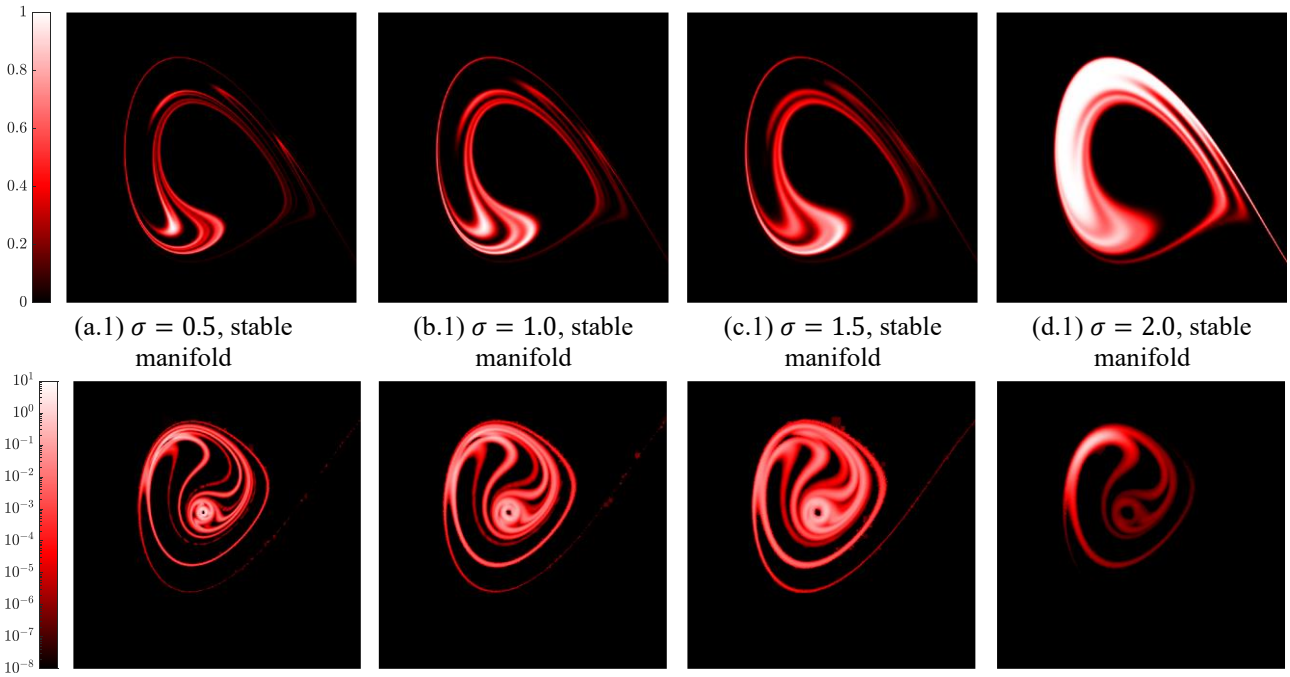

(a.1) $\sigma = 0.5$, stable manifold | (b.1) $\sigma = 1.0$, stable manifold | (c.1) $\sigma = 1.5$, stable manifold | (d.1) $\sigma = 2.0$, stable manifold

(a.2) $\sigma = 0.5$, unstable manifold | (b.2) $\sigma = 1.0$, unstable manifold | (c.2) $\sigma = 1.5$, unstable manifold | (d.2) $\sigma = 2.0$, unstable manifold

Fig. 8 – Dependency of the stable manifold observable g_{W_s} and unstable manifold distribution f_{W_u} onto the noise intensity σ, in $(w_1, \dot{w}_1) \in \{-2,3\} \otimes \{-70,60\}$. $A = 17V$, $\Omega = 15$, $\xi = 0.03$

Finally, Fig. 9 depicts the saddle support (highlighted in red) for increasing noise levels σ. The stochastic bifurcation is visually identified as the resonant attractor becomes enveloped by the unstable manifold. This is consistent with the established understanding that such bifurcations can be defined by a sudden, radical change in the character of stochastic attractors and their basins. The merging of an attractor with a manifold, as can be observed, is a key topological feature of this phenomenon.

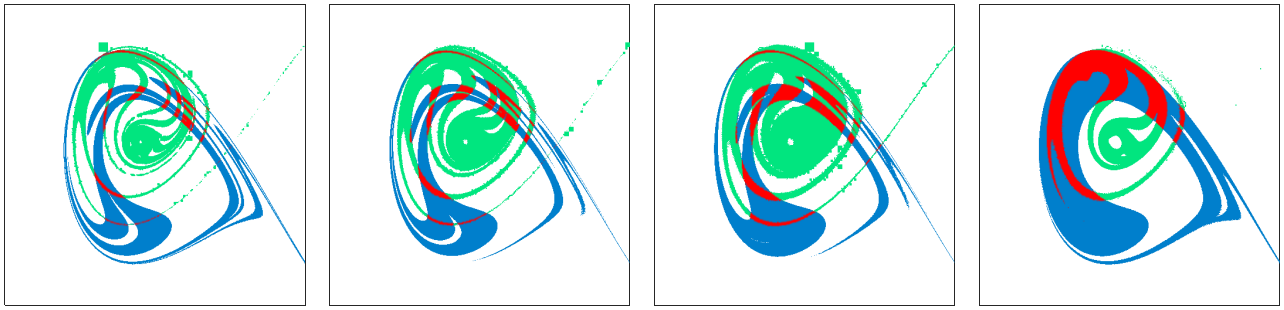

a) $\sigma = 0.5$ | (b) $\sigma = 1.0$ | (c) $\sigma = 1.5$ | (d) $\sigma = 2.0$

Fig. 9 – Stable (blue) and unstable (green) manifolds superposition (in red), marking the saddle for different noise intensity σ, in $(w_1, \dot{w}_1) \in \{-2,3\} \otimes \{-70,60\}$. $A = 17V$, $\Omega = 15$, $\xi = 0.03$

The final analysis examines the influence of parametric uncertainty on the stable and unstable manifolds, as well as the flow structures in phase space. The damping ratio is assumed to be uniformly distributed, $\xi \sim U(a, 0.05)$. Four cases were investigated, with $a \in \{0.04,\ 0.03,\ 0.02,\ 0.01\}$. Basins and escape regions are reported in Fig. 10. For details of the numerical strategy, please refer to [17]. As the parameter a moves from 0.04 to 0.01, both basins and escape regions diffuse over the phase-space, corresponding to an increasing uncertainty of the outcome for a given initial condition.

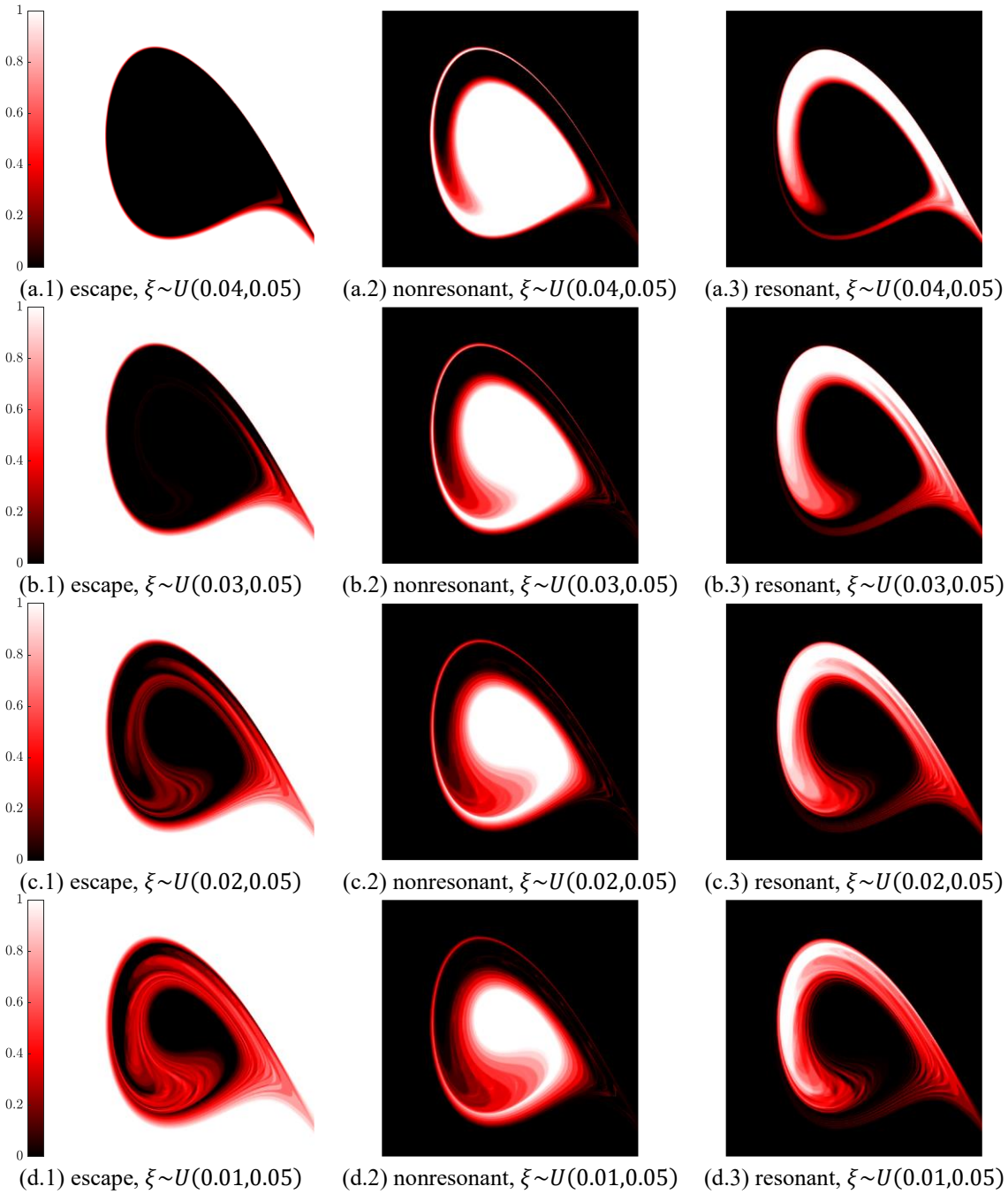

Fig. 10 – Deterministic system with parametric uncertainty. Mean basins and mean escape regions for varying damping ratio ξ distributions in $(w_1, \dot{w}_1) \in \{-2,3\} \otimes \{-70,60\}$. $A = 17V$, $\Omega = 15$

The effects of parametric uncertainty on the stable and unstable manifolds of the deterministic system are depicted in Fig. 11. The interactions and mixing of the manifolds are illustrated in Fig. 12.

As uncertainty increases, the mean structures diffuse across the phase space, leading to greater complexity in the flow structure. For the lower uncertainty case, shown in Fig. 11 (a) and Fig. 12(a), the unstable manifold remains relatively simple, while the stable manifold is already diffused over a large region. Additionally, a diffusion of the saddle is observed in Fig. 12(a), highlighted in red. This reflects the basins' topology in Fig. 10(a), with large nondeterministic regions. The unstable manifolds, Fig. 11(2), present regions of high probability, with the support of the nonresonant attractor localized in a small region, due to the damping ratio ξ distribution, while the support of the resonant attractor spreads along a curve. The stable manifold, Fig. 11(1), develops a complex structure as uncertainty increases, with growing regions of intersection, as observed in Fig. 12(d). Lastly, discontinuities are observed in all cases, a spurious result due to the adopted n-point collocation discretization of the probability space $(\mathbb{L}, P_\lambda)$. This effect is known in the uncertainty quantification literature, motivating the development of adaptative discretization techniques of the probability space [66].

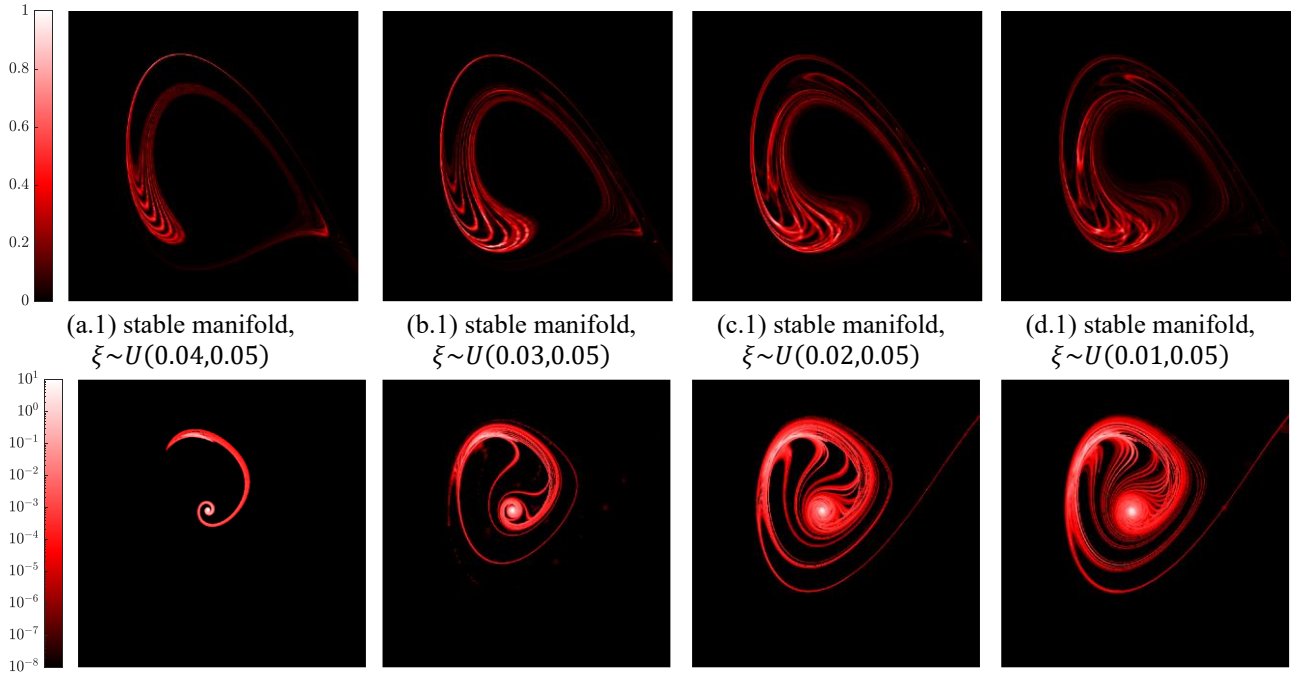

(a.1) stable manifold, $\xi \sim U(0.04,0.05)$ | (b.1) stable manifold, $\xi \sim U(0.03,0.05)$ | (c.1) stable manifold, $\xi \sim U(0.02,0.05)$ | (d.1) stable manifold, $\xi \sim U(0.01,0.05)$

(a.2) unstable manifold, $\xi \sim U(0.04,0.05)$ | (b.2) unstable manifold, $\xi \sim U(0.03,0.05)$ | (c.2) unstable manifold, $\xi \sim U(0.02,0.05)$ | (d.2) unstable manifold, $\xi \sim U(0.01,0.05)$

Fig. 11 – Dependency of the stable and unstable manifolds' distributions on the damping ratio ξ distributions, in $(w_1, \dot{w}_1) \in \{-2,3\} \otimes \{-70,60\}$. $A = 17V$, $\Omega = 15$

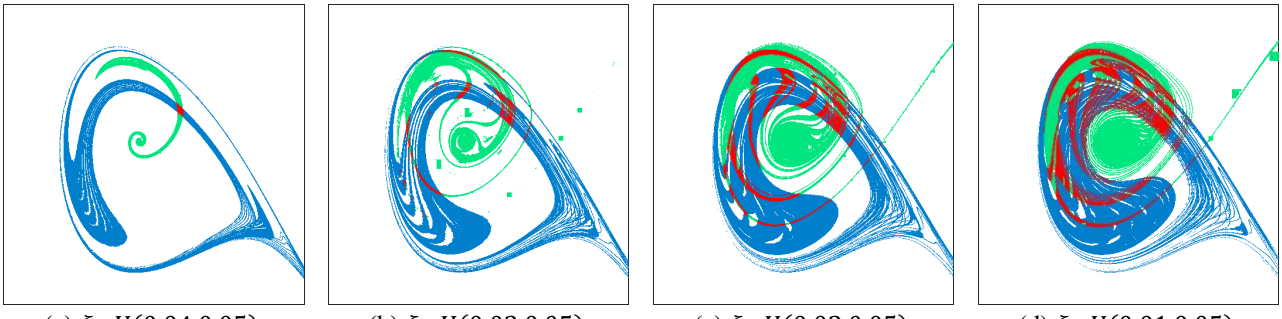

(a) $\xi \sim U(0.04,0.05)$ | (b) $\xi \sim U(0.03,0.05)$ | (c) $\xi \sim U(0.02,0.05)$ | (d) $\xi \sim U(0.01,0.05)$

Fig. 12 – Stable (blue), and unstable (green) manifolds superposition (in red), marking the saddle for different damping ratio distributions ξ, in $(w_1, \dot{w}_1) \in \{-2,3\} \otimes \{-70,60\}$. $A = 17V$, $\Omega = 15$

4 Final remarks

This work explored the definitions of stable and unstable manifolds within the framework of measurable dynamics of nondeterministic systems. We defined transfer and composition operators for nondeterministic systems and revisited the classical Ulam discretization. Our analysis demonstrated that the resulting distributions on unstable manifolds reside in the space of piecewise constant functions over the phase-space partition. This clarification was essential to establish that the corresponding dual space comprises the constant unitary functions over the same partition – a key result for defining observables on stable manifolds. Building on this foundation, we integrated definitions of invariant manifolds for nondeterministic dynamics with the spectral theory of Markov operators. By defining a one-way boundary over attractors' regions, an open-flow dynamical system and corresponding transfer operators $\overline{\mathcal{P}}_t$ and $\overline{\mathcal{K}}_t$ were constructed. Their properties were investigated, and the existence of distributions of unstable manifolds f_{W_u} and observables of stable manifolds g_{W_s}, considering both weak convergence and strong convergence in measure, was demonstrated. The main result characterizes f_{W_u} and g_{W_s} as eigenfunctions of $\overline{\mathcal{P}}_t$ and $\overline{\mathcal{K}}_t$, respectively, each associated with a dominant real eigenvalue $|\mu| < 1$. Leveraging their duality relation, a discretization strategy based on the Ulam method was developed. This approach introduces a parameter c to define the open-flow operator, enabling the simultaneous approximation of both f_{W_u} and g_{W_s}.

To demonstrate the proposed methodology and investigate the effects of noise and parametric uncertainties on invariant manifolds, we applied it to an electrically actuated microarch. The study encompassed deterministic, stochastic, and random-parameter regimes. Transfer operators were constructed using the discretization strategies previously outlined. The analysis revealed intricate dependencies between the invariant manifolds, noise intensity, system parameters, and the saddle point dynamics. A key finding is that the loss of convergence probability under noise is associated with an expansion of the stable manifold over the stochastic basin and a concurrent merging of the unstable manifold with the attractor, forming a quasi-stationary distribution with dominant eigenvalue almost one. These results imply that long transient solutions can be anticipated when the stable manifold occupies extensive regions of the phase space.

Future research directions include, but are not limited to, applications of this theory to other problems of interest, such as fast-slow dynamics or engineering models. From a computational perspective, the classical Ulam discretization, while a powerful general strategy, suffers from slow convergence and high computational costs. We aim to explore more complex discretized spaces inspired by Koopman theory to address these limitations.

Acknowledgments

The authors also acknowledge the financial support of the Brazilian research agencies, CNPq [grant numbers 304364/2023-1 and 401514/2022-6], FAPERJ-CNE [grant number E-

26/201.033/2022], FAPERJ Nota 10 [grant number E-26/200.357/2020] and CAPES [finance code 001 and 88881.310620/2018-01].

Declaration of Competing Interest

The authors declare that they have no known competing financial interests or personal relationships that could have appeared to influence the work reported in this paper.

Data Availability

The datasets generated during and/or analyzed during the current study are available from the corresponding author on reasonable request.

References

1. Guckenheimer, J., Holmes, P.: Nonlinear Oscillations, Dynamical Systems, and Bifurcations of Vector Fields. Vol. 42, Springer New York, New York, NY (1983)
2. Thompson, J.M.T., Stewart, H.B.: Nonlinear Dynamics and Chaos. Wiley, Chichester, England (2002)
3. Nayfeh, A.H., Balachandran, B.: Applied Nonlinear Dynamics. Wiley, New York (1995)
4. Farjami, S., Kirk, V., Osinga, H.M.: Computing the Stable Manifold of a Saddle Slow Manifold. SIAM J. Appl. Dyn. Syst. 17, 350–379 (2018). https://doi.org/10.1137/17M1132458
5. Guckenheimer, J., Krauskopf, B., Osinga, H.M., Sandstede, B.: Invariant manifolds and global bifurcations. Chaos An Interdiscip. J. Nonlinear Sci. 25, 097604 (2015). https://doi.org/10.1063/1.4915528
6. Guckenheimer, J., Vladimirsky, A.: A Fast Method for Approximating Invariant Manifolds. SIAM J. Appl. Dyn. Syst. 3, 232–260 (2004). https://doi.org/10.1137/030600179
7. Hatjispyros, S.J., Kaloudis, K.: A Bayesian nonparametric approach to the approximation of the global stable manifold. Chaos. 29, (2019). https://doi.org/10.1063/1.5122187
8. Brunton, S.L., Budišić, M., Kaiser, E., Kutz, J.N.: Modern Koopman Theory for Dynamical Systems. SIAM Rev. 64, 229–340 (2022). https://doi.org/10.1137/21M1401243
9. Dellnitz, M., Junge, O.: On the approximation of complicated dynamical behavior. SIAM J. Numer. Anal. 36, 491–515 (1999). https://doi.org/10.1137/S0036142996313002
10. Bollt, E.M., Santitissadeekorn, N.: Applied and Computational Measurable Dynamics. Society for Industrial and Applied Mathematics, Philadelphia, PA (2013)

11. Dellnitz, M., Hohmann, A.: A subdivision algorithm for the computation of unstable manifolds and global attractors. Numer. Math. 75, 293–317 (1997). https://doi.org/10.1007/s002110050240

12. Dellnitz, M., Hohmann, A., Junge, O., Rumpf, M.: Exploring invariant sets and invariant measures. Chaos An Interdiscip. J. Nonlinear Sci. 7, 221–228 (1997). https://doi.org/10.1063/1.166223

13. Dellnitz, M., Froyland, G., Junge, O.: The algorithms behind GAIO — set oriented numerical methods for dynamical systems. In: Fiedler, B. (ed.) Ergodic Theory, Analysis, and Efficient Simulation of Dynamical Systems. pp. 145–174. Springer Berlin Heidelberg, Berlin, Heidelberg (2001)

14. Yue, X.-L., Xu, Y., Xu, W., Sun, J.-Q.: Global invariant manifolds of dynamical systems with the compatible cell mapping method. Int. J. Bifurc. Chaos. 29, 1950105 (2019). https://doi.org/10.1142/S0218127419501050

15. Yue, X.-L., Xu, Y., Xu, W., Sun, J.-Q.: Probabilistic response of dynamical systems based on the global attractor with the compatible cell mapping method. Phys. A Stat. Mech. its Appl. 516, 509–519 (2019). https://doi.org/10.1016/j.physa.2018.10.034

16. Benedetti, K.C.B., Gonçalves, P.B., Lenci, S., Rega, G.: Global analysis of stochastic and parametric uncertainty in nonlinear dynamical systems: adaptative phase-space discretization strategy, with application to Helmholtz oscillator. Nonlinear Dyn. 111, 15675–15703 (2023). https://doi.org/10.1007/s11071-023-08667-5

17. Benedetti, K.C.B., Gonçalves, P.B., Lenci, S., Rega, G.: Parameter uncertainty and noise effects on the global dynamics of an electrically actuated microarch. J. Micromechanics Microengineering. 33, 064001 (2023). https://doi.org/10.1088/1361-6439/acceb0

18. Junge, O.: An adaptive subdivision technique for the approximation of attractors and invariant measures: proof of convergence. Dyn. Syst. 16, 213–222 (2001). https://doi.org/10.1080/14689360110060708

19. Dellnitz, M., Junge, O.: An adaptive subdivision technique for the approximation of attractors and invariant measures. Comput. Vis. Sci. 1, 63–68 (1998). https://doi.org/10.1007/s007910050006

20. Han, Q., Xu, W., Yue, X.-L.: Stochastic response analysis of noisy system with non-negative real-power restoring force by generalized cell mapping method. Appl. Math. Mech. 36, 329–336 (2015). https://doi.org/10.1007/s10483-015-1918-6

21. Han, Q., Xu, W., Sun, J.-Q.: Stochastic response and bifurcation of periodically driven nonlinear oscillators by the generalized cell mapping method. Phys. A Stat. Mech. its Appl. 458, 115–125 (2016). https://doi.org/10.1016/j.physa.2016.04.006

22. Yue, X.-L., Xiang, Y., Zhang, Y., Xu, Y.: Global analysis of stochastic bifurcation in shape memory alloy supporter with the extended composite cell coordinate system method. Chaos An Interdiscip. J. Nonlinear Sci. 31, 013133 (2021). https://doi.org/10.1063/5.0024992

23. Lindner, M., Hellmann, F.: Stochastic basins of attraction and generalized committor functions. Phys. Rev. E. 100, 022124 (2019). https://doi.org/10.1103/PhysRevE.100.022124

24. Klünker, A., Padberg-Gehle, K., Thiffeault, J.-L.: Open-flow mixing and transfer operators. Philos. Trans. R. Soc. A Math. Phys. Eng. Sci. 380, 8–10 (2022). https://doi.org/10.1098/rsta.2021.0028

25. Froyland, G., Stancevic, O.: Escape rates and Perron-Frobenius operators: Open and closed dynamical systems. Discret. Contin. Dyn. Syst. - Ser. B. 14, 457–472 (2010). https://doi.org/10.3934/dcdsb.2010.14.457

26. Dellnitz, M., Junge, O.: Almost Invariant Sets in Chua's Circuit. Int. J. Bifurc. Chaos. 07, 2475–2485 (1997). https://doi.org/10.1142/S0218127497001655

27. Froyland, G., Dellnitz, M.: Detecting and locating near-optimal almost-invariant sets and cycles. SIAM J. Sci. Comput. 24, 1839–1863 (2003). https://doi.org/10.1137/S106482750238911X

28. Froyland, G.: Statistically optimal almost-invariant sets. Phys. D Nonlinear Phenom. 200, 205–219 (2005). https://doi.org/10.1016/j.physd.2004.11.008

29. Froyland, G., Padberg, K.: Almost-invariant sets and invariant manifolds — Connecting probabilistic and geometric descriptions of coherent structures in flows. Phys. D Nonlinear Phenom. 238, 1507–1523 (2009). https://doi.org/10.1016/j.physd.2009.03.002

30. Froyland, G.: Unwrapping eigenfunctions to discover the geometry of almost-invariant sets in hyperbolic maps. Phys. D Nonlinear Phenom. 237, 840–853 (2008). https://doi.org/10.1016/j.physd.2007.11.004

31. Arnold, L.: Random Dynamical Systems. Springer Berlin Heidelberg, Berlin, Heidelberg (1998)

32. Yagasaki, K.: Melnikov processes and chaos in randomly perturbed dynamical systems. Nonlinearity. 31, (2018). https://doi.org/10.1088/1361-6544/aab89f

33. Lu, K., Wang, Q.: Chaos in differential equations driven by a nonautonomous force. Nonlinearity. 23, 2935–2975 (2010). https://doi.org/10.1088/0951-7715/23/11/012

34. Lu, K., Wang, Q.: Chaotic behavior in differential equations driven by a Brownian motion. J. Differ. Equ. 251, 2853–2895 (2011). https://doi.org/10.1016/j.jde.2011.05.032

35. Ashwin, P.: Minimal attractors and bifurcations of random dynamical systems. Proc. R. Soc. London. Ser. A Math. Phys. Eng. Sci. 455, 2615–2634 (1999). https://doi.org/10.1098/rspa.1999.0419

36. Padberg, K., Thiere, B., Preis, R., Dellnitz, M.: Local expansion concepts for detecting transport barriers in dynamical systems. Commun. Nonlinear Sci. Numer. Simul. 14, 4176–4190 (2009). https://doi.org/10.1016/j.cnsns.2009.03.018

37. Dellnitz, M., Klus, S., Ziessler, A.: A set-oriented numerical approach for dynamical systems with parameter uncertainty. SIAM J. Appl. Dyn. Syst. 16, 120–138 (2017). https://doi.org/10.1137/16M1072735

38. Gerlach, R., Koltai, P., Dellnitz, M.: Revealing the intrinsic geometry of finite dimensional invariant sets of infinite dimensional dynamical systems. (2019). https://doi.org/10.48550/arXiv.1902.08824

39. Ziessler, A., Dellnitz, M., Gerlach, R.: The numerical computation of unstable manifolds for infinite dimensional dynamical systems by embedding techniques. SIAM J. Appl. Dyn. Syst. 18, 1265–1292 (2019). https://doi.org/10.1137/18M1204395

40. Gerlach, R., Ziessler, A., Eckhardt, B., Dellnitz, M.: A set-oriented path following method for the approximation of parameter dependent attractors. SIAM J. Appl. Dyn. Syst. 19, 705–723 (2020). https://doi.org/10.1137/19M1247139

41. Ding, J., Li, T.Y.: Markov finite approximation of Frobenius-Perron operator. Nonlinear Anal. Theory, Methods Appl. 17, 759–772 (1991). https://doi.org/10.1016/0362-546X(91)90211-I

42. Ding, J., Du, Q., Li, T.Y.: High order approximation of the Frobenius-Perron operator. Appl. Math. Comput. 53, 151–171 (1993). https://doi.org/10.1016/0096-3003(93)90099-Z

43. Jin, C., Ding, J.: A linear spline Markov approximation method for random maps with position dependent probabilities. Int. J. Bifurc. Chaos. 30, 2050046 (2020). https://doi.org/10.1142/S0218127420500467

44. Bangura, R.M., Jin, C., Ding, J.: The norm convergence of a least squares approximation method for random maps. Int. J. Bifurc. Chaos. 31, 2150068 (2021). https://doi.org/10.1142/S0218127421500681

45. Benedetti, K.C.B., Gonçalves, P.B., Lenci, S., Rega, G.: Influence of uncertainties and noise on basins/attractors topology and integrity of Duffing oscillator. Int. J. Non. Linear. Mech. 159, 104594 (2024). https://doi.org/10.1016/j.ijnonlinmec.2023.104594

46. Klus, S., Koltai, P., Schütte, C.: On the numerical approximation of the Perron-Frobenius and Koopman operator. J. Comput. Dyn. 3, (2015). https://doi.org/10.3934/jcd.2016003

47. Yue, X., Wang, Y., Han, Q., Xu, Y., Xu, W.: Transient responses of nonlinear dynamical systems under colored noise. EPL (Europhysics Lett. 127, 24004 (2019). https://doi.org/10.1209/0295-5075/127/24004

48. Yue, X., Wang, Y., Han, Q., Xu, Y., Xu, W.: Probabilistic response and stochastic bifurcation in a turbulent swirling flow. J. Comput. Nonlinear Dyn. 14, (2019). https://doi.org/10.1115/1.4044500

49. Han, Q., Xu, W., Hao, H., Yue, X.: Global analysis of stochastic systems by the digraph cell mapping method based on short-time gaussian approximation. Int. J. Bifurc. Chaos. 30, 2050071 (2020). https://doi.org/10.1142/S0218127420500716

50. Belardinelli, P., Lenci, S.: A first parallel programming approach in basins of attraction computation. Int. J. Non. Linear. Mech. 80, 76–81 (2016). https://doi.org/10.1016/j.ijnonlinmec.2015.10.016

51. Belardinelli, P., Lenci, S.: An efficient parallel implementation of cell mapping methods for MDOF systems. Nonlinear Dyn. 86, 2279–2290 (2016). https://doi.org/10.1007/s11071-016-2849-3

52. Siettos, C., Russo, L.: A numerical method for the approximation of stable and unstable manifolds of microscopic simulators. Numer. Algorithms. 89, 1335–1368 (2022). https://doi.org/10.1007/s11075-021-01155-0

53. Patsatzis, D., Fabiani, G., Russo, L., Siettos, C.: Slow invariant manifolds of singularly perturbed systems via physics-informed machine learning. SIAM J. Sci. Comput. 46, C297–C322 (2024). https://doi.org/10.1137/23M1602991

54. Yue, X., Jing, X., Liu, X., Li, Y., Xu, Y.: Parameter identification of dynamical systems based on short-term prediction by the generalized cell mapping method with deep learning. Nonlinear Dyn. 113, 4031–4044 (2025). https://doi.org/10.1007/s11071-024-09943-8

55. Yue, X.-L., Cui, S.-P., Zhang, H., Sun, J.-Q., Xu, Y.: Generalized cell mapping method with deep learning for global analysis and response prediction of dynamical systems. Int. J. Bifurc. Chaos. 31, 1–20 (2021). https://doi.org/10.1142/S0218127421502291

56. Yue, X., Cui, S., Pei, B., Xu, Y.: Responses of stochastic dynamical systems by the generalized cell mapping method with deep learning. Int. J. Non. Linear. Mech. 147, 104190 (2022). https://doi.org/10.1016/j.ijnonlinmec.2022.104190

57. Yue, X.-L., Zhang, H., Li, Y., Xu, Y.: Global dynamics and noise-induced transitions for a two-dimensional panel system in subsonic flow. Acta Mech. Sin. 40, 523472 (2024). https://doi.org/10.1007/s10409-024-23472-x

58. Ochoa, D.E., Poveda, J.I.: Robust global optimization on smooth compact manifolds via hybrid gradient-free dynamics. Automatica. 171, 111916 (2025). https://doi.org/10.1016/j.automatica.2024.111916

59. Kaszás, B., Haller, G.: Globalizing manifold-based reduced models for equations and data. Nat. Commun. 16, 5722 (2025). https://doi.org/10.1038/s41467-025-61252-9

60. Chekroun, M.D., Liu, H., Wang, S.: Approximation of Stochastic Invariant Manifolds. Springer International Publishing, Cham (2015)

61. Lasota, A., Mackey, M.C.: Chaos, Fractals, and Noise. Vol. 97, Springer New York, New York, NY (1994)

62. Ding, J., Yien Li, T., Zhou, A.: Finite approximations of Markov operators. J. Comput. Appl. Math. 147, 137–152 (2002). https://doi.org/10.1016/S0377-0427(02)00429-6

63. Hsu, C.S.: Cell-to-Cell Mapping. Vol. 64, Springer New York, New York, NY (1987)

64. Sun, J.-Q., Hsu, C.S.: The generalized cell mapping method in nonlinear random vibration based upon short-time gaussian approximation. J. Appl. Mech. 57, 1018–1025 (1990). https://doi.org/10.1115/1.2897620

65. Jaeger, L., Kantz, H.: Homoclinic tangencies and non-normal Jacobians — Effects of noise in nonhyperbolic chaotic systems. Phys. D Nonlinear Phenom. 105, 79–96 (1997). https://doi.org/10.1016/S0167-2789(97)00247-9

66. Le Maître, O.P., Knio, O.M.: Spectral Methods for Uncertainty Quantification. Springer, Dordrecht (2010)